Marine Geology 492 (2026) 107679

Contents lists available at ScienceDirect

Marine Geology

journal homepage: www.elsevier.com/locate/margo

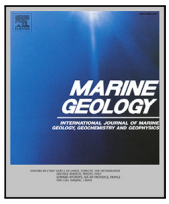

Research article

Shoreline evolution in a low-lying coastal region under anthropogenic influence

Matteo Meli [a,*], Enrica Vecchi [b], Claudia Romagnoli [a]

[a] Department of Biological, Geological and Environmental Sciences, University of Bologna, Piazza di Porta San Donato 1, Bologna, 40126, Italy
[b] Department of Civil, Environmental Engineering and Architecture, University of Cagliari, Via Marengo 2, Cagliari, 09123, Italy

ARTICLE INFO

Editor: Nadia Senechal

Dataset link: https://doi.org/10.5281/zenodo.14849128

Keywords:
Satellite-derived shoreline
Coastal processes
Sea-level rise
Anthropogenic impacts
Interannual variability
Emilia-romagna

ABSTRACT

This study aims to reconstruct and analyze shoreline evolution along the highly urbanized Emilia-Romagna coast (Italy) over the period 1984–2023 using satellite-derived shorelines. Landsat and Sentinel-2 imagery were processed with the CoastSat toolbox, and shoreline positions were corrected for tide and wave setup before deriving yearly averages from 2,200 transects. While the spatial resolution of yearly-averaged SDS is lower than that of conventional techniques, this approach enables, for the first time in this region, the reconstruction of shoreline dynamics as a continuous time series spanning interannual to multi-decadal scales. Results highlight substantial spatial and temporal variability across the shoreline, driven by the interplay of natural processes and anthropogenic interventions such as coastal defenses, repeated nourishments, and sediment extraction. Despite ongoing sea-level rise and subsidence, most of the coast exhibits stability or net advancement, largely maintained through human interventions. The resulting dataset provides one of the most temporally extensive records of shoreline variability for the Emilia-Romagna coast and represents a valid basis for future monitoring and coastal management.

1. Introduction

Sandy shorelines, covering roughly one-third of the Earth's ice-free coastline (Luijendijk et al., 2018), are among the most dynamic and ecologically significant environments (Schlacher et al., 2007; Castelle and Masselink, 2023). They serve as natural buffers against increasingly frequent and intense storms (Arkema et al., 2013), while providing critical socio-economic benefits, including tourism, recreation, and coastal ecosystem services (Martínez et al., 2007; Ghermandi and Nunes, 2013). However, climate change, rising sea levels, and declining sediment supply are accelerating coastal erosion, posing severe environmental and socioeconomic challenges (Syvitski et al., 2022; IPCC, 2023). These impacts threaten both developed and developing regions, affecting coastal settlements, infrastructure, and livelihoods (Alexandrakis et al., 2015).

The shoreline, defined as the intersection of sea and land surfaces, is a key indicator of coastal change, with its position and evolution closely tied to the interaction of multiple Earth system components (IPCC, 2023). The analysis of shoreline variability and trends provides a fundamental basis for effective coastal management and protection design, as it enables the assessment of climate change-related drivers influencing coastline evolution and future projections (Toimil et al., 2020). However, the shoreline is inherently a time-dependent (dynamic) feature governed by the interaction of non-linear processes operating across multiple temporal and spatial scales, increasing uncertainty in future coastal hazard assessments (Barnard et al., 2019). At decadal and multi-decadal scales, sediment supply and redistribution (i.e., alongshore gradients in longshore transport), relative sea-level change, climate-related factors, and anthropogenic impacts are the main drivers of shoreline changes (Zhang et al., 2004; Mentaschi et al., 2018).

Due to this dynamic nature, a range of coastal monitoring techniques exists, each with differing levels of applicability and accuracy (Boak and Turner, 2005; Castelle et al., 2021; Vecchi et al., 2021). Traditional approaches include GNSS-RTK surveys, aerial photography, and, more recently, LiDAR surveys, which can provide very high-resolution three-dimensional reconstructions of coastal changes over the past decades. However, these methods often have limited temporal or spatial coverage, and continuous multi-decadal records remain scarce, primarily due to practical and methodological constraints. In this context, satellite-derived coastal imagery has emerged as a valuable complement to in situ and airborne observations, offering consistent data coverage since the mid-1980s and enabling shoreline analysis across both short-term (daily to interannual) and long-term (decadal to multi-decadal) scales (Turner et al., 2021).

Shoreline detection along sandy coastlines has been applied, for

* Corresponding author.
E-mail address: matteo.meli7@unibo.it (M. Meli).

https://doi.org/10.1016/j.margeo.2025.107679
Received 7 July 2025; Received in revised form 9 October 2025; Accepted 2 November 2025
Available online 19 November 2025

instance, to monitor repeated nourishments and estimate their effects, evaluate the impact of stormy periods, and assess long-term shoreline trends and interannual variability (Luijendijk et al., 2018; Turner et al., 2021; Castelle et al., 2021, 2024; Vos et al., 2023a; Almar et al., 2023). Over recent decades, satellite missions like Landsat and Sentinel-2 have played a crucial role in providing consistent and multi-decadal shoreline datasets. Landsat imagery, available since the launch of Landsat 5 in 1984, offers global coverage with a spatial resolution of 30 m for multispectral bands and 15 m for the panchromatic band in Landsat 7, 8, and 9. Sentinel-2, operational since 2015, provides a higher spatial resolution of 10 m for visible and near-infrared bands and a global revisit time of 5 days since 2017. In some applications, pansharpening techniques have been used to enhance the spatial resolution of Landsat multispectral imagery by fusing it with the higher-resolution panchromatic band Zhang et al. (2023). These advancements in satellite imagery now enable the generation of time series of satellite-derived shorelines (SDS), offering multi-decadal records of variability, trends, and changes with a cross-shore accuracy of approximately 10 m on microtidal beaches (Bishop-Taylor et al., 2019; Vos et al., 2019a; Cuttler et al., 2020). This capability is crucial for long-term coastal monitoring and management, particularly at the local scale (e.g., from tens of kilometers down to hundreds of meters), where the continuous interplay between anthropogenic and natural factors adds complexity to coastal evolution.

From an operational perspective, different proxies can be used to represent the shoreline, including the wet/dry line, vegetation line, high-water line, or geomorphic features such as dune and cliff toes (Boak and Turner, 2005). Each proxy has specific advantages and limitations, depending on the scale of analysis and the data available. In the context of satellite-derived approaches, the sand–water limit is the most widely adopted indicator, owing to its strong spectral contrast; however, it presents some intrinsic limitations. In particular, the shoreline is extracted from single images acquired under specific tidal and hydrodynamic conditions, making the application of tidal corrections essential. Global tide models (e.g., TPXO (Egbert and Erofeeva, 2002), FES2014 (Lyard et al., 2021)) are often preferred, but their coarse resolution can compromise the reliability of the final products (Sun et al., 2022). Conversely, local tide gauges provide higher temporal accuracy but introduce other challenges, such as the need for consistent vertical referencing (Wang et al., 2023; Vos et al., 2023b; Vecchi, 2023; Aschenneller et al., 2024) and the limited spatial representativeness of single stations, which may not capture variability across broader regions or even at smaller spatial scales, such as in bays or gulfs (Devlin et al., 2019; Meli et al., 2021; Ramos-Alcántara et al., 2022; Pan et al., 2024). Additionally, the local beach slope directly affects the land–water interface through wave run-up, with gentle profiles amplifying this effect (Di Luccio et al., 2018). These aspects highlight that SDS-based shoreline detection, although powerful, requires careful treatment of hydrodynamic and topographic influences to ensure robust results.

The typical approach for analyzing multiple SDS datasets is the "Baseline and Transects" method (Himmelstoss et al., 2024). This method involves defining a baseline, usually aligned with the general orientation of the coastline in the study area, and generating several cross-shore transects where the intersection points of each shoreline are automatically computed (Gómez-Pazo et al., 2022). Unlike the conventional approach, which focuses on comparing subsequent time periods, an averaged shoreline can be reconstructed by computing the averaged intersection points from all available SDS over a specific time frame and connecting them along closely spaced transects (Vos et al., 2023b; Castelle et al., 2021, 2024).

In this study, SDS positions along the Emilia-Romagna coast in the northern Adriatic Sea (Fig. 1) were reconstructed using the CoastSat toolbox (Vos et al., 2019b) to analyze shoreline changes over the period 1984–2023. While CoastSat is typically used to extract high-frequency SDS data, matching the satellite revisit period under low cloud cover conditions (García-Rubio et al., 2015; Hagenaars et al., 2018), annual means are computed here to better capture long-term trends and reduce intra-annual noise. Currently, the available data on shoreline evolution along the Emilia-Romagna coast consist of a series of aerial photographs, GNSS surveys, and LiDAR datasets (https://geoportale.regione.emilia-romagna.it), each capturing a single moment in time. Despite their high spatial resolution and accuracy, these snapshots cannot be fully representative of long-term behavior and lack temporal continuity. In parallel, recent advances in sub-pixel shoreline extraction have improved the effective spatial precision of optical sensors, enabling reconstructions over multi-decadal periods at regional (Konlechner et al., 2020; Bishop-Taylor et al., 2021; Vos et al., 2023a) and local scales (García-Rubio et al., 2015; Almonacid-Caballer et al., 2016; Castelle et al., 2021). Thus, the aim of this study is to explore whether SDS data can reliably represent continuous interannual to multi-decadal shoreline evolution and to what extent they can reveal the influence of natural and anthropogenic drivers on coastal dynamics across space and time.

2. Study area

The Emilia-Romagna (hereafter ER) coast extends approximately 130 km in a NW-SE orientation, south of the Po River Delta (Fig. 1a). Since the second half of the 20th century, the ER coast has significantly developed as a tourist destination, becoming a key contributor to the national economy (Lorito et al., 2010). Consequently, urban settlements have widely expanded, leading to the coastal area losing its natural character, except for a few protected natural areas and reserves of ecological value that have persisted following extensive land reclamation of marshy and lagoon areas over the last few centuries (Bruno et al., 2024). Nowadays, beaches along the ER coast are predominantly occupied by touristic and recreational structures, often built very close to or even replacing dune ridges. The entire coastline is characterized by low-gradient, dissipative beaches, mostly composed of fine to medium sand Aguzzi et al. (2016). On average, the beach width (excluding infrastructure) exceeds 70 m along 35% of the total coastline, ranges between 70 and 50 m for 19%, and is less than 50 m for 36% (Regione Emilia–Romagna, 2022). However, the average height is below 1.5 m for 45% of the beaches, exposing large portions of the coast to flooding from extreme sea levels due to relevant storms (see, for instance, Ciavola et al. (2007), Perini et al. (2011). Indeed, most of the ER coastal plain does not exceed 2 m above mean sea level, with some parts of the hinterland currently lying below mean sea level (Calabrese et al., 2024).

In terms of wave climate, the region is characterized by low-energy waves (Aguzzi et al., 2016). The most frequent conditions exhibit wave heights of up to 1 m and periods ranging from 5 to 7 s, primarily associated with directions from 90° N (Romagnoli et al., 2021). Storms primarily impact the coast from either the NE (Bora wind) or the SE (Sirocco wind) (Lionello et al., 2012). Tidal range , typically 0.3 m during neap tides and up to 0.8 m during spring tides, classifies the ER coast as a microtidal environment (Davies, 1964). However, storm surge levels caused by wind-driven water piling and low barometric pressure can nearly double the tidal range, with extreme sea levels of approximately 1 m occurring within 1- to 10-year return periods (Masina and Ciavola, 2011), leading to extensive coastal inundation and erosion.

Recent estimates of local sea-level rise indicate a rate of 3.0 ± 0.5 mm/yr over the last three decades (Meli et al., 2023, 2025). However, the contribution of subsidence, in terms of vertical land movements along the coastal plain, has significantly amplified relative sea-level rise, with localized variations ranging from approximately 55% to 640% (Meli et al., 2025). Indeed, the region lies within a foredeep basin affected by natural subsidence, resulting from both tectonic activity and the compaction of Quaternary alluvial deposits (Carminati and Di Donato, 1999; Amorosi et al., 2004; Teatini et al., 2011; Bruno

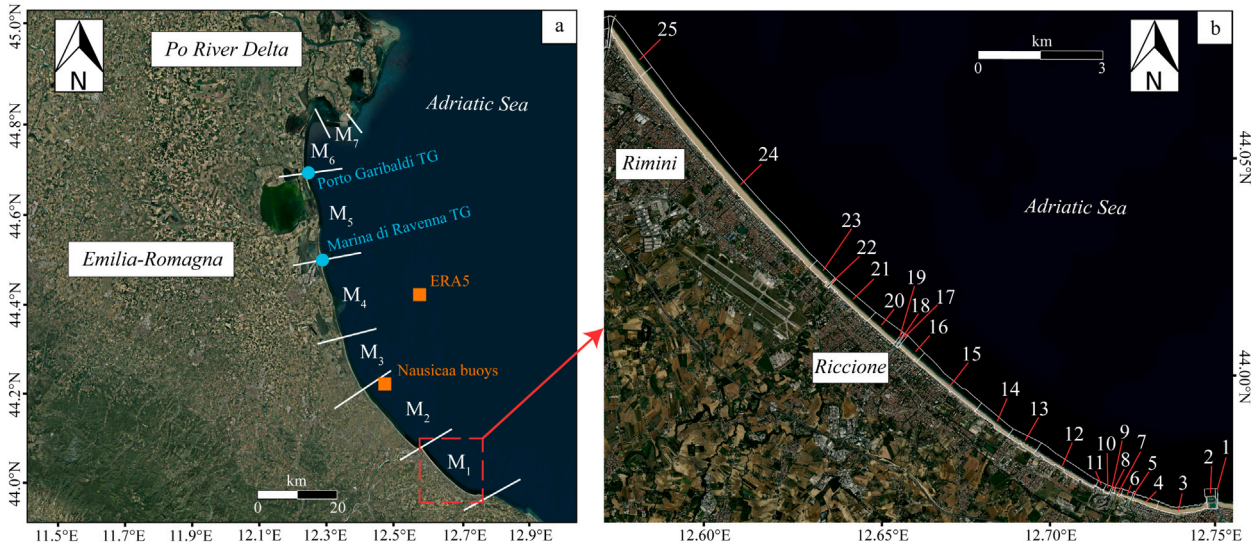

Fig. 1. (a) The study area, divided into seven macrocells (M_i) as delineated by Regione Emilia–Romagna (2014), faces the northern Adriatic Sea. The location of the considered tide gauges are marked with cyan dots, while the position of the Nausicaa buoys and the ERA5 grid point are indicated by an orange square. (b) A detailed view of the M_1 (see also the red hatched square in panel (a) for the location along the ER coast) with the associated coastal management cells (from 1 to 25).

et al., 2020), with rates ranging from 1 to 2 mm/yr across the coastal plain and peaking in the Po River Delta (Gambolati and Teatini, 1998; Teatini et al., 2011). A marked increase in subsidence trends occurred in the second half of the 20th century due to anthropogenic activities, such as groundwater withdrawal and gas extraction (Carminati and Martinelli, 2002; Teatini et al., 2006), with rates locally exceeding natural subsidence by an order of magnitude (Bitelli et al., 2000) and reaching values of up to 15–20 mm/yr in some areas. However, following the adoption of regional policies limiting groundwater withdrawal, subsidence has gradually decreased in recent decades (Marcaccio and Mazzei, 2023), although high rates (up to 10 mm/yr) are still observed in specific areas of the coastal plain Meli et al. (2025). The combined effect of subsidence, sea-level rise, and urbanization has resulted in erosion and increased exposure to coastal flooding along most of the ER coast (Perini et al., 2016). This situation is further exacerbated by the progressive decline in fluvial sediment supply. Indeed, primarily due to anthropogenic interventions in catchment areas, fluvial transport has drastically decreased over the 20th century (Preti et al., 2009; Meli and Romagnoli, 2022), leaving the coast largely deprived of riverine sediment inputs. Consequently, a large portion of the coast is artificially maintained in equilibrium through various defense strategies, including both “hard” (defense structures) and “soft” (nourishment) measures (Aguzzi et al., 2016, 2020).

Defense structures such as breakwaters, groynes, and revetments have been widely employed since the second half of the twentieth century along a significant portion of the coastline, covering 57% of its total length; however, they have led to beach stiffening and interference with natural sedimentary dynamics (Regione Emilia–Romagna, 2022). In the last four decades, however, beach nourishment interventions have been preferred and regularly implemented not only at the local scale (“maintenance replenishment” by using sediment extracted from nearby coastal tracts or construction excavations, or derived from beach cleaning operations) but also on a regional scale. Major campaigns (in the order of 2–3 million cubic meters each) were conducted in 2002, 2007, 2016, and 2022, increasingly using offshore sands following the discovery of marine deposits suitable for this purpose (Preti et al., 2009; Correggiari et al., 1996). Thus, coastal dynamics along the ER coast are largely influenced by anthropogenic factors. A significant portion of local shoreline variability is driven by the interaction between coastal structures and the longshore current, which predominantly flows in a southeast-to-northwest direction or, in some areas, in the opposite direction (Preti et al., 2009). This effect is particularly evident in various coastal locations, where the shoreline gradually advances on the updrift side of long piers and jetties, while the downdrift side experiences sediment starvation and shoreline retreat Preti et al. (2009), Aguzzi et al. (2016, 2020).

3. Materials and methods

The analysis along the ER coast was conducted by dividing it into macrocells, each ranging from 15 to 30 km in length (Fig. 1a) and coastal management cells (Fig. 1b and Tab. S1), as defined in Regione Emilia–Romagna (2014). In detail, the ER coast is generally split using this approach, as each macrocell, from the first to the sixth (hereon M_1 to M_6, respectively), is separated from the others by the presence of harbors, long piers, or river mouths. This leads to the creation of specific, virtually separated coastal dynamics for each macrocell, with related predominant longshore currents and sediment input/loss redistribution. It should be noted that the ER coast also includes a seventh macrocell (the southern part of the Po River Delta; see also Fig. 1a), which is not considered here due to the lack of data for the analysis and its complex hydrodynamics. Further fragmentation within each macrocell has led to the establishment of management cells, as the presence of hard defense structures has further altered sediment transport dynamics along the coastal stretches, thereby requiring different management approaches (Aguzzi et al., 2016).

3.1. CoastSat

The extraction of SDS along the ER coast was performed using the open-source CoastSat Python toolbox (Vos et al., 2019b), which is currently among the best-performing and most competitive SDS algorithms available (Vos et al., 2023b). This toolbox, publicly available at https://github.com/kvos/CoastSat, allows for the selection of a region of interest and automatically delineates the position of the instantaneous sand–water limit using Landsat (5–9) and Sentinel-2 images, downloaded through the Google Earth Engine Application Programming Interface (Gorelick et al., 2017). Shoreline extraction is based on the top-of-atmosphere multi-spectral bands (blue, green, red, near-infrared, and short-wave infrared). The images are first classified to separate water and land pixels, maximizing the variance by selecting the Otsu

threshold (Otsu, 1979) using the modified normalized water index. Then, the sand–water limit is extracted using a subpixel resolution border segmentation method (Cipolletti et al., 2012).

A dataset of 50 m-spaced cross-shore transects (Fig. 2a), aligned with the beach profile (local orientation), was automatically generated using a Python script. This resulted in the creation of approximately 2200 individual transects covering around 110 km of sandy coastline under analysis. Then, the cross-shore distance along each transect was computed for all the extracted shorelines over the period 1984–2023. All transects remained fixed throughout the 40-year analysis period. This allowed the extraction of shoreline positions (coordinates) from the meter-scale distances measured along the transects, corresponding to the intersection between each transect and the instantaneous sand–water limit.

Differences in revisit time and the resolution/quality of the available missions, combined with the additional constraint of variable cloud cover, resulted in varying frequencies of the automatically extracted shorelines. Moreover, the application of the CoastSat despiking algorithm, which removes outliers caused by false detections, led to a further reduction in the number of valid observations. Despite spatial heterogeneity along the coast, the total number of valid instantaneous shoreline detections retained after preprocessing from 1984 to 2023 ranged from 1000 to approximately 1300 across the study area. Hence, exploiting the large number of available instantaneous shorelines to compute an annually averaged position has resulted in both noise reduction and increased reliability of the final product. Indeed, the instantaneous assessment of the shoreline, observed for instance from satellite images, single GNSS surveys, aerial photographs, LiDAR, or topo-bathymetric campaigns, each representing a single acquisition at a given moment, is strongly affected by the conditions at the time of acquisition, preventing continuous analysis of shoreline evolution in the mid to long-term. For this reason, resampling at a lower temporal resolution has been preferred here to overcome the effects of various processes acting at higher temporal frequencies, allowing for a more robust temporal analysis and a clearer view of coastline evolution.

All valid observations extracted and processed with CoastSat were first automatically converted into monthly means. Subsequently, the residual effect of the mean seasonal cycle (see also Section 4.1) for each specific macrocell, after partial reduction through the applied corrections (see Section 3.2), was removed from each individual month. This prevented the introduction of bias in years when observations from all months were not available and aimed to eliminate the influence of intra-annual variability. Finally, the data were converted to yearly means and linearly interpolated. The latter was performed both temporally, for gaps of up to 1 year, and spatially, for gaps corresponding to a single missing lateral transect, ensuring continuity and consistency in the dataset.

3.2. Corrections

The effect of oscillating water levels represents one of the main sources of error in SDS, as the extracted time series are based on the instantaneous position of the sand–water limit. Indeed, applying the correction for local tide excursions to the SDS time series is considered crucial and strongly recommended (Vos et al., 2019b), especially in locations with flatter beach profiles, such as the ER coast. Moreover, the effect of wave setup (the sustained increase in nearshore water levels caused by breaking waves) and wave runup (the back-and-forth movement of the sand–water limit due to waves breaking and moving inland) should be taken into account, as their correction might improve the accuracy of the SDS time series (Vitousek et al., 2023). Wave runup, however, cannot usually be corrected unless the phase of specific waves is known at the moment the satellite images were taken.

Following the procedure described in Vos et al. (2023b), the extracted instantaneous cross-shore positions (Δx) for the ER coast were corrected for the corresponding tide level (ζ) at a specific time (t_i):

$$\Delta x_{\zeta}(t_i) = \Delta x(t_i) + \frac{\zeta(t_i)}{\tan\beta_f(M_i)} \quad (1)$$

where Δx_{ζ} is the cross-shore position corrected for tide, and $\tan\beta_f$ is the beach-face slope (i.e., the area between mean high water springs and mean sea level, as defined by Vos et al. (2020)), averaged over time for each coastal macrocell (M_i). The local ζ time series was reconstructed by considering tide gauge (TG) data (refer to Fig. 1a for location) from Marina di Ravenna, sourced from the GESLA-3 database (Haigh et al., 2023), and from Porto Garibaldi, sourced from Arpae-Dext3r (https://simc.arpae.it/dext3r/). At the time of the analysis, data from TGs were available from January 1975 to May 2021 for Marina di Ravenna, updated to December 2023 by integrating data from the Italian TG network (https://www.mareografico.it/), and from May 2009 to December 2023 for Porto Garibaldi. However, due to strong discontinuities and the massive presence of suspicious and flagged data, observations prior to 2000 in the Marina di Ravenna TG were removed. Data from both TGs were resampled from subhourly to hourly resolution by averaging all time samples that fall within a ± 30 min window of each specific hour. In order to remove both the influence of interannual variability and local vertical land movements from the two TG signals, each year within the time series was detrended by subtracting the corresponding annual mean (Muis et al., 2020). The two TG time series were then averaged, and the mean was removed to center the data at zero; the missing data (less than 0.11% of the total) were linearly interpolated to avoid gaps. At this stage, a complete time series of hourly sea-level variability representative of the ER coast was achieved (Fig. 2b), covering the period from 01 January 2000 (00:00:00) to 31 December 2023 (23:00:00). Thus, this time series was used to achieve local ζ by performing harmonic analysis and prediction with the UTide algorithm (Codiga, 2011). The parameters for the computation were set as the robust fitting method, latitude 44.5° N, and a Rayleigh criterion minimum of 0.95. Finally, the coefficients from the harmonic analysis enabled the modeling of the tidal signal for the period prior to the available observations, matching the CoastSat SDS period, i.e., from 01 January 1984 to 31 December 1999 (Fig. 2b).

In order to assess the $\tan\beta_f$ parameter for each macrocell along the ER coast, height/depth data (also known as topo-bathymetric data) acquired by the ER Regional Agency for Prevention, Environment, and Energy (Arpae) were taken into account. Topo-bathymetric data have been acquired approximately every six years (i.e., 1984, 1993, 2000, 2006, 2012, 2018) through dedicated monitoring campaigns (IDROSER, 1983, 1996; ARPA, 2002; Preti et al., 2009; Aguzzi et al., 2016, 2020). These data consist of a dense network of elevation points relative to the local zero (mean sea level), collected using a dual-frequency GNSS system in RTK-OTF mode for the emerged beach (up to the dune or streets/urban settlements) and a multibeam echosounder (single-beam prior to 2006) for the submerged portions (down to a depth of approximately -10 m). In this study, elevation maps with a 1 m-grid spacing resolution (Fig. 2a) for the six macrocells and the six topo-bathymetric campaigns were computed using the Delaunay algorithm (Delaunay, 1934) in QGIS. Subsequently, $\tan\beta$ values at each grid point were derived from the slope maps. The spatial average of $\tan\beta_f$ was then calculated using only the values within the contours of the mean high water spring tide and mean sea level, which were estimated based on the reconstructed ζ parameter described above to be approximately 40 cm and 0 cm above mean sea level (white area in Fig. 2a), respectively. The spatially averaged $\tan\beta_f$ for each macrocell is found to be strongly consistent over time, i.e., showing no substantial changes in beach-face slope values across the six campaigns within a 1σ range (also coherent for the entire intertidal zone, down to the mean low water spring), with values of 0.032 ± 0.004 (M_1), 0.023 ± 0.001 (M_2), 0.027 ± 0.002 (M_3), 0.028 ± 0.004 (M_4), and 0.030 ± 0.002

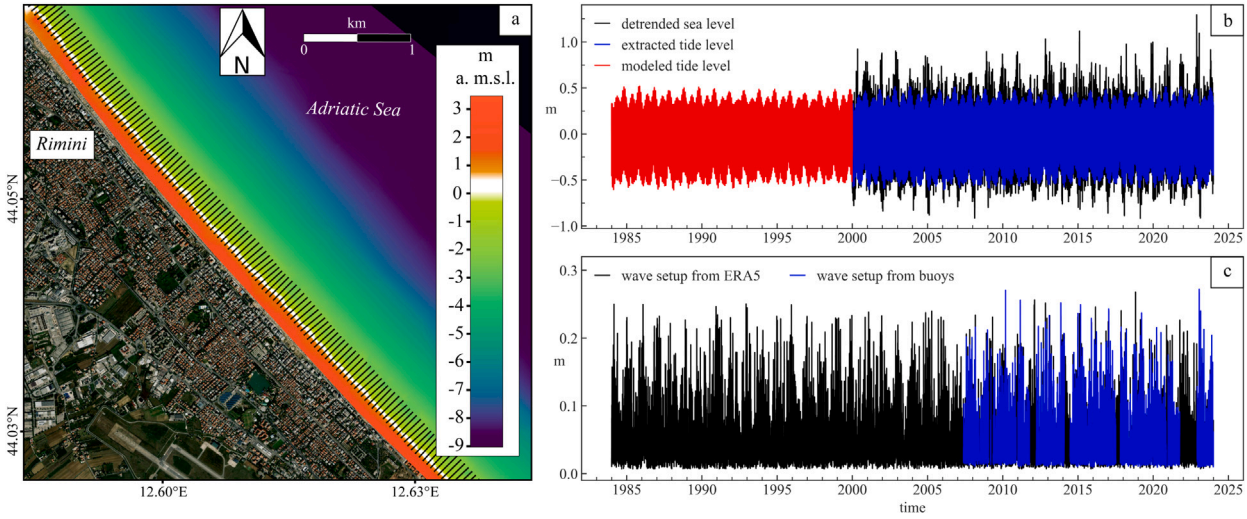

Fig. 2. (a) Detailed view of Cell 24 within M_1 (see Figs. 1a and b for location), showing 50 m-spaced cross-shore transects (black lines), employed for the SDS CoastSat extractions, and the 1-m grid elevation map (in m above mean sea level) derived from the 2018 topo-bathymetric survey (Aguzzi et al., 2020); the white area indicates the beach face used for estimating the $\tan\beta_f$ parameter (see Section 3.2 for details). (b) The reconstructed hourly local sea level (black line), with trend and interannual variability removed, and the corresponding extracted tide component (blue line), spanning from 01 January 2000 to 31 December 2023; the red line indicates the modeled tide level over the period of CoastSat data set not covered by local sea level data (01 January 1984–31 December 1999). (c) The reconstructed local wave setup time series from both observations (Nausicaa buoys) and reanalysis data (ERA5).

(for both M_5 and M_6). Thus, these values have been used as the $\tan\beta_f$ correction parameters for their respective macrocells.

On top of the tidal correction, cross-shore positions corrected for wave setup (Δx_η) were achieved following (Vos et al., 2023b):

$$\Delta x_\eta(t_i) = \Delta x_\zeta(t_i) + \frac{\eta(t_i)}{\tan\beta_f(M_i)} \tag{2}$$

where (η) is the locally reconstructed wave setup parameter (Fig. 2c). Since the entire ER coast is characterized by strongly dissipative conditions, assessed here to have an Iribarren number (Battjes, 1974) of less than 0.1, a slope-independent parameterization of wave setup has been considered, as suggested by Stockdon et al. (2006):

$$\eta(t_i) = 0.016(H_0 L_0)^{1/2} \tag{3}$$

where H_0 and L_0 are the deep-water wave height and wavelength, respectively. These two parameters were achieved by averaging data from both the closest grid point from the ERA5 global reanalysis (Hersbach et al., 2020) and local observations from the Nausicaa-I and Nausicaa-II buoys from Arpae-Dext3r (locations in Fig. 1a). In detail, hourly time series of H_0 and wave period (T) are available for the entire period of interest within the reanalysis (i.e., from 01 January 1984 to 31 December 2023) and for the periods from 23 May 2007 to 05 October 2021 and from 01 December 2022 to 31 December 2023 for Nausicaa-I and Nausicaa-II, respectively. The L_0 parameter was then computed using the linear dispersion relationship:

$$L_0 = \frac{gT^2}{2\pi} \tag{4}$$

Before averaging the time series and linearly interpolating the few remaining gaps, data from reanalysis and observations were checked by comparison and filtered by removing spikes or suspicious values. In terms of similarity, the filtered series show a very high agreement, providing $RMSE$ values of 0.014 and R^2 of 0.84. Thus, the η parameter for the entire period not covered by observations (that is, from 1984 to 2006) was assumed to be reliable based on the reanalysis.

3.3. Time-series analysis

The temporal variability of the yearly reconstructed shorelines was analyzed at the cell scale by averaging the trends calculated for each individual transect within the cell. This approach overcomes the issue of averaging portions of the coast with different characteristics (e.g., varying orientation, dynamics, presence or absence of hard structures, and human interventions), as each cell is independently represented by its specific setting. Cells associated with harbors, small pocket beaches, and fluvial inlets or channels were excluded from the analysis due to insufficient or missing data, as well as to avoid bias from local effects, following the procedure described in Section 3.1. Consequently, only sandy coastal cells with adequate data coverage were considered, ensuring that each computed time series accurately represents cell dynamics over the 40-year analysis period. Following this approach, 74 out of 110 cells were considered (see also Tab. S1 for details), covering approximately 96% of the ER coast.

The long-term linear trends over the 40 years under analysis were assessed using the non-parametric Theil–Sen estimator (Sen, 1968). Statistical significance at the 95% confidence level was evaluated by applying the non-parametric Mann–Kendall test, adapted for autocorrelated data (Hamed and Ramachandra Rao, 1998). To avoid underestimating trend errors linked to autocorrelation in the data, the trend uncertainty was adjusted using the autoregressive parameter at lag 1.

The time series for the period 1993–2020 of local geocentric sea level (Gregory et al., 2019), which represents the sea-level variation with respect to the Earth's center of mass, was retrieved from (Meli et al., 2025). To extend these observations back to 1984, the starting date for CoastSat imagery, data from the Marina di Ravenna TG were incorporated. In order to ensure consistency with the geocentric series, the TG data were first corrected for local vertical land movements, as described by Meli and Romagnoli (2022) and Zerbini et al. (2021). Subsequently, corrections for both the inverse barometer effect and glacial isostatic adjustment were applied following (Meli, 2024). The two datasets were then concatenated by aligning their temporal means and resampled from monthly to yearly means. Finally, the time series was extended up to 2023 in accordance with the procedure described in Meli et al. (2025).

Data about subsidence evolution were retrieved from (Aguzzi et al., 2020) for the periods 1984–1987 and 1987–1992, from Arpae-Geoportal (https://servizi-gis.arpae.it/Html5Viewer/index.html?locale=it-IT&viewer=Geoportal.Geoportal) for 1992–2000 and 2002–2006, and from (Meli et al., 2025) for 2006–2011, 2011–2016, and 2016–2021. Because data from (Aguzzi et al., 2020) consist of

scattered, single measurements along the ER shoreline (from the so-called Coastal Geodetic Network) based on in situ leveling, these values were spatially interpolated to ensure complete coverage of the entire coastline. Moreover, since data from both (Aguzzi et al., 2020) and Arpae-Geoportal represent trends, these were assumed to remain constant over each selected period and were converted into time series. The years 2001 and 2021–2023 were also assumed to be consistent with values from the periods 2002–2006 and 2016–2020, respectively. Thus, a 40-year subsidence time series was computed by averaging all available data within each cell.

To isolate the influence of relative sea-level (RSL) variations on shoreline evolution, a set of theoretical shorelines was reconstructed for each of the 74 cells over the 40-year period under analysis. In this framework, the RSL combines the geocentric sea level with the historical subsidence observed for each cell. By applying a generic slope-displacement relation

$$\Delta x(t_i) = -\frac{\zeta(t_i) + \eta(t_i)}{\tan\beta(cell_i)} \tag{5}$$

the extent of each shoreline's advancement or retreat was computed solely as a geometric response to RSL changes. In this case, however, the $\tan\beta$ parameter was derived for each cell by considering the entire active coastal profile (from the upper beach down to the depth of closure), rather than focusing solely on the beach face, following the same procedure described in Section 3.2. Incorporating the full profile is essential for capturing the broader magnitude and rate of shoreline change driven by long-term processes such as RSL rise. The achieved $\tan\beta$ values for each cell (see Tab. S1) are generally 5 to 10 times lower than those related to the foreshore portion of the beach, as expected, and align with the single value (0.0062) provided by Athanasiou et al. (2019).

The removal of any theoretical shoreline evolution from its original signal within each cell isolates all aspects other than RSL. Once the theoretical signal, representing the effects of RSL, is removed, the remaining component, indicative of morphodynamic contributions, was further analyzed. These signals from all cells were then decomposed using 1000 iterations of the non-parametric Ensemble Empirical Mode Decomposition (Wu and Huang, 2009), considering only the residual signals (i.e., after removing the oscillatory modes). This approach enables the observation of the non-linear long-term shoreline trend at each cell, solely driven by morphodynamic adjustment to natural and anthropogenic processes.

Available data on nourishment and sediment extraction interventions at the cell scale, as well as the presence or absence of hard defense structures, have been incorporated into the analysis to find possible correlations. A detailed database on nourishments and extractions at the coastal cell scale has been made available by Arpae. This database is periodically updated, providing information on timing, exact location, and intervention magnitude (m^3 of sediment extracted or provided), with records dating back to the 1970s. However, not all interventions are documented, as some smaller-scale nourishments and extractions remain, nowadays, unknown. Information about hard defense structures is provided through the so-called 'Defense Structures Catalog' (https://datacatalog.regione.emilia-romagna.it/catalogCTA/dataset), issued by the ER Regional Administration. This consists of a set of shapefiles containing digitally mapped hard structures extracted from aerial photographs. Since the construction dates of most structures are unknown, the adopted strategy involves periodically generating shapefiles based on aerial images taken at different times, allowing for the identification of a time window in which a specific structure was built or re-adapted.

At last, a comparison was performed between the SDS-derived shorelines and pre-existing coastal datasets for the ER coast over the same period. These datasets consist of: (i) six manually mapped shorelines, developed and distributed by the ER Regional Administration (https://datacatalog.regione.emilia-romagna.it/catalogCTA/group/costa), based on single aerial photographs and considered representative of the ER shoreline for the years 1996, 1998, 2005, 2014, 2019, and 2020; and (ii) three shoreline datasets (https://www.arpae.it/it/dati-e-report/dati-ambientali), produced by Arpae through the extraction of the zero-meter contour line above mean sea level from the GNSS topo-bathymetric surveys described above. The comparison was conducted using the same cross-shore transects employed for SDS extraction, focusing on the entire regional coast as a whole. Specifically, the intersection distances of the shorelines generated in this study (i.e., the union of each macrocell's shoreline) were compared with those from the ER and Arpae datasets for the corresponding years.

4. Results

4.1. Annual-averaged shorelines

The interpretation of the obtained annually-averaged shoreline positions requires some consideration. The potential variability of the shoreline induced by high-frequency processes might lead to substantial divergences, as it has been assessed by modifying the generic slope-displacement relation (i.e., Eq. (5), but with the use of the $\tan\beta_f(M_i)$ parameter). Following this relationship, the combined effect of tide and wave setup, relative to the average slope of the ER beach-face, might result in a variability of approximately 20 m in each direction (landward and seaward), leading to a total range of ca. 40 m in shoreline position on an hourly scale (Fig. 3a). This aspect cannot be properly accounted for in aerial images, as exact information about the timing of acquisition is almost always unavailable. The complexity also arises at the monthly resolution (Fig. 3a), where marked asymmetric seasonality appears and might lead to divergences ranging from approximately 4.8 m landward to 1.2 m seaward. This asymmetry, primarily driven by the effect of wave setup, is eventually reflected in the annual average (Fig. 3a), quantified here as -1.6 ± 0.2 m (i.e., landward). This means that, on average, the yearly mean shorelines produced in this study are generally shifted seaward due to the application of the corrections.

Besides the combined effect of tide and wave setup, at the intra-annual scale, the shoreline is subjected to strong variability induced by several other factors, such as changes in sea level properties (e.g., variations in water level due to density, atmospheric pressure, and oceanic circulation) and fluvial liquid and sediment supply. These factors result in significant seasonality (Fig. 3b), quantified here as an amplitude range exceeding 9 m (averaged across the entire ER coast). Its removal was enabled in this study, thanks to the high frequency of information provided by the CoastSat toolbox. Maximum shoreline advancement is observed in late summer (from the end of August to early September), while a retreat pattern occurs in winter, as expected considering the common wave climate in the area.

For these reasons, the direct comparison between the processed SDS and the pre-existing shorelines available for the ER coast may be affected by inconsistencies. The latter datasets, while offering very high spatial resolution, are influenced by high-frequency processes and lack both the hydrodynamic corrections applied to the SDS and temporal continuity. Overall, the comparison shows moderate variability: in some sectors, shorelines coincide, whereas in others, discrepancies reach several tens of meters (Fig. 4). On average, the pre-existing shorelines differ from the SDS-derived shorelines by 14.4 ± 10.2 m (1σ). The median difference is 13.9 m, with an interquartile range of 9.4 m, indicating a stable central tendency and a mild right skew with occasional large positive deviations. This asymmetry is consistent with the observed extremes (mean minimum of −34.7 m and mean maximum of 139.5 m). In this context, positive (negative) extremes refer to discrepancies seaward (landward) of the SDS-derived shorelines produced in this study relative to the pre-existing datasets. This is consistent with the previously observed seaward shift associated with the application of corrections. However, these extremes can be treated as outliers, as the majority of the comparisons (5th–95th percentile

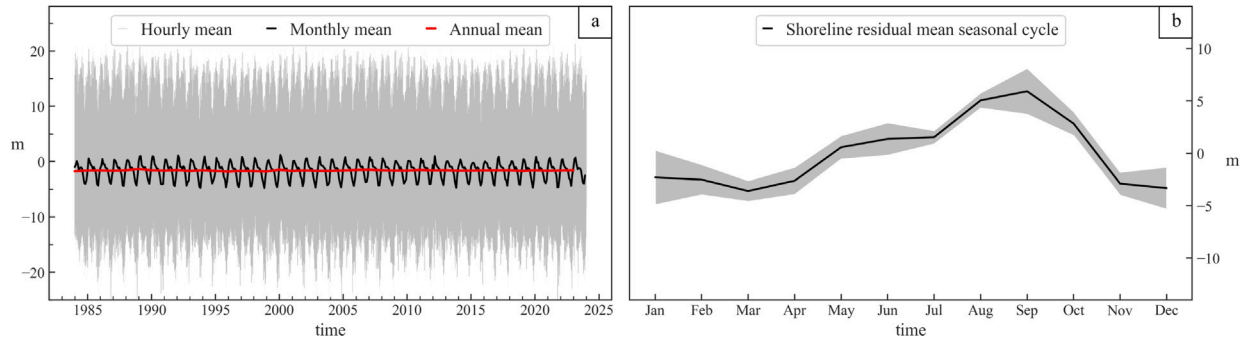

Fig. 3. (a) The averaged geometric response of the ER shoreline to the combined effects of tide and wave setup, shown at hourly (gray), monthly (black), and annual (red) resolution. Negative (positive) values on the y-axis indicate a potential retreat (advancement) of the shoreline due to these components. (b) The removed residual seasonal cycle, averaged across the entire ER coast (black solid line) with its 1σ (gray shaded area), remaining after the application of corrections (see Section 3.2). As for panel (a), positive (negative) values in the seasonal signal correspond to an advancement (retreat) of the shoreline.

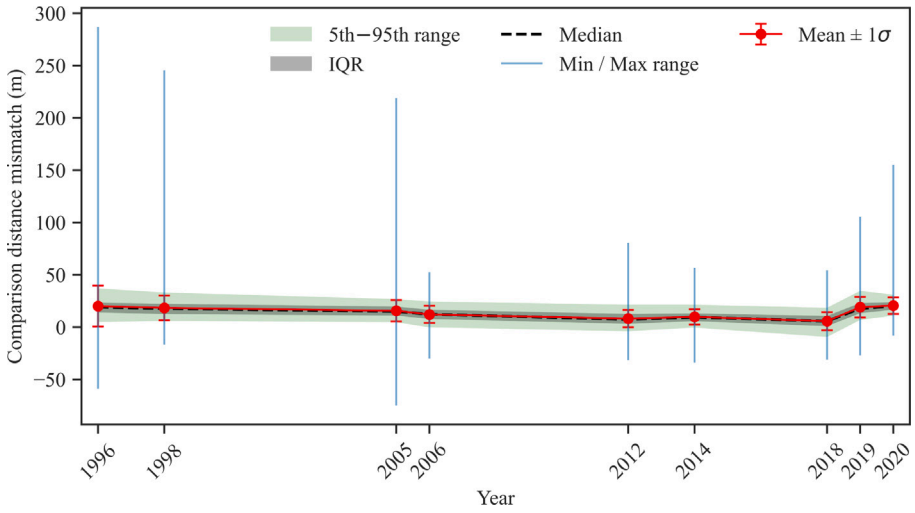

Fig. 4. Discrepancies between regionally averaged SDS-derived shorelines (this study) and the nine pre-existing shoreline datasets along the ER coast. Positive (negative) values (m) denote seaward (landward) offsets relative to the SDS-derived shoreline. The mean discrepancy over the entire coast for a given year is shown as red dots with 1σ whiskers; the median is the dashed black line, with the interquartile range (IQR, gray area) and the 5th–95th percentile range (green area). Minimum-to-maximum discrepancies for each year are indicated by the vertical blue line.

range; Fig. 4) are confined around the median, with a total range of approximately 25 m. Moreover, a thorough examination of the results reveals that the highest extreme values and 1σ spreads are associated with the 1996–2014 period, indicating higher variability within the Landsat datasets. For this period, however, RMSE (Root Mean Square Error) values fall within the pixel resolution of the images, ranging from 11.6 m to 28.1 m, while the same does not hold for the Sentinel-2 datasets, which show RMSE values of 10.4 m, 21.5 m, and 22.1 m for the years 2018, 2019, and 2020, respectively. While the mean errors for the Sentinel-2 period are similar to those of Landsat, the 1σ spread is generally lower (7.9–9.9 m), indicating a more consistent error distribution. Notably, comparing a single satellite-derived shoreline with contemporaneous or slightly delayed ground-truth can yield significantly higher accuracy, often reaching sub-pixel levels (Zollini et al., 2023; Brown et al., 2025). In this study, however, the situation differs, given that SDS shorelines are averaged over a year and the comparison relies on available ground-truth data from a single point in time, chosen to be representative of the entire year. Considering this approach, along with the observed average errors and RMSE values, the extracted shoreline is considered reliable within the expected accuracy.

In terms of trends calculated at the cell scale (Fig. 5), over the period 1984–2023, the long-term evolution of annually averaged shorelines reveals substantial variability along the ER coast, differing both within each macrocell and among adjacent cells. As evidenced in Fig. 5, the majority of the considered cells (59) exhibited a trend ranging between −1 and 1 m/yr, among which 20 cells (3, 12, 14, 16, 20, 30, 35, 43, 48, 52, 54, 58, 60, 72, 76, 79, 88, 102, 105, and 107) show trends that are not statistically significant (Fig. 6 and S1–S5). Generally, a progradational tendency prevails (43 cells) at the coastal scale, with a maximum value of 4.2 m/yr observed in cell 100 (within M_5), while an erosional pattern is identified in 31 cells, with a maximum value of −9.8 m/yr in cell 94 (M_5).

4.2. Interannual shoreline variability

Despite being fundamental information, long-term trends may not fully capture coastal evolution, as each cell is inherently influenced by multiple non-linear processes. A key insight provided by the SDS analysis is the ability to examine coastal evolution as a time series. This approach allows, for the first time along the ER coast, both the visualization and quantification of the complex and diverse non-linearities that characterize each coastal tract. Indeed, as shown in Fig. 6 for M_1 (refer to the Figures in the Supplementary Materials for the other macrocells), despite their spatial proximity, each cell exhibits a distinct non-linear evolution over time. Furthermore, the widespread 1σ variance in some cases highlights the persistence of complex shoreline evolution variability even within a single cell (e.g., cells 3, 4, 12, and 15 in M_1), suggesting that even the finer parceling adopted with

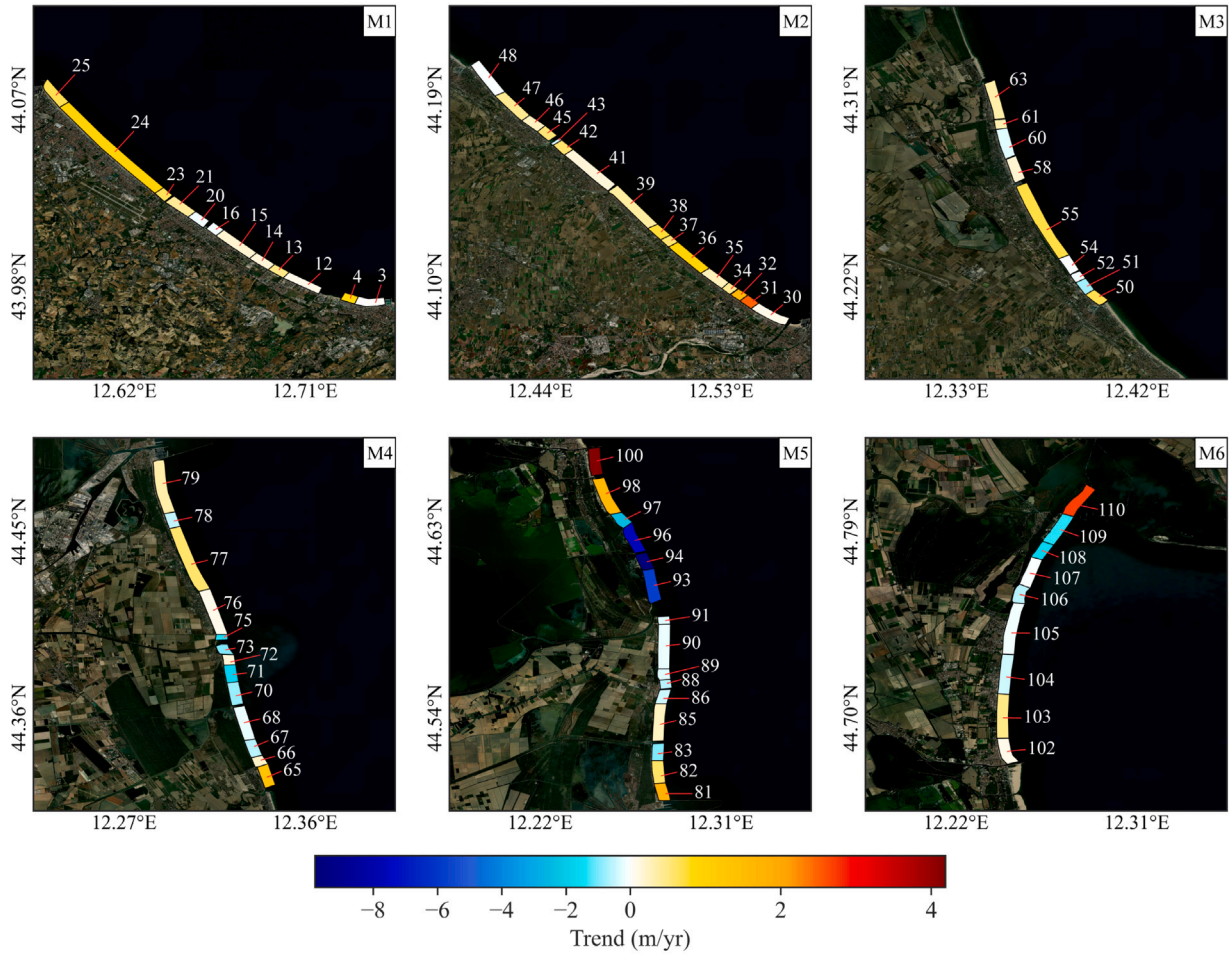

Fig. 5. Linear trend for each cell within the six macrocells over the 40-year analysis period. Positive (negative) values indicate a progradational (erosional) pattern in m/year.

cells may not be sufficient to fully capture or isolate local complex dynamics.

Generally, the observed non-linear tendencies are consistent with previous studies based on volumetric assessments averaged over multiple topo-bathymetric campaigns. These studies indicate an overall progradational or stable trend over time, which is attributed to the adopted defense strategies that maintain most of the coast in an artificially balanced condition (Preti et al., 2009; Armaroli et al., 2012; Aguzzi et al., 2016, 2020; Regione Emilia–Romagna, 2022). Indeed, repeated and high-volume (over 20 $m^3 \times 10^3$) nourishment interventions have been carried out along the regional coast, usually within specific cells. The dumped sediment was, in some cases, of internal provenance, i.e., derived from cells characterized by coastal accumulations (e.g., cells 3 and 24 within M_1; Fig. 6), and, in other cases, of external provenance, mostly from offshore deposits since 2007. A consistent pattern between larger-scale nourishment interventions and prompt shoreline advancement appears in cells 12, 14, 15, 37, 38, 47, 50–51, 54, 60–61, 72, 77, and 83, as well as an increasing advancement or, at least, relative stabilization of the shoreline position after repeated nourishments (i.e., cells 20, 32, 35–36, 42–43, 45–46, 66–67, 85, 105, 108–109). Conversely, in some cells (e.g., 71, 76, 78 in macrocell M_4, and 96, 97 in M_5), the shoreline position does not exhibit significant changes or trend variations, despite repeated nourishment interventions. This suggests that, in these areas, sediment inputs may be insufficient to counteract local erosional processes or that the reworking of deposited material occurs at a rate that prevents long-term accumulation. These sectors are indeed among the most critical along the regional coast in terms of erosion and vulnerability (Aguzzi et al., 2016). In other coastal areas, where the accumulation of sediment is favored, repeated sediment extractions (on the order of several tens of m^3 each) are carried out (such as in cells 3, 24, 58, 79, 81, 100, and 110). This results in localized shoreline retreat on a yearly basis, which is generally reabsorbed quickly, making some of these areas key sediment sources for nourishment interventions in other coastal cells.

Without anthropogenic modifications, shoreline trends would have been significantly different, considering the virtual sediment loss estimated at several million cubic meters (Preti et al., 2009) caused by subsidence and generalized sediment starvation. Additionally, RSL rise would have resulted in substantial land loss, as pointed out in the theoretical shoreline evolution within each cell (Fig. 6), where the potential landward shift, albeit non-linear, would have remained persistent over time. The morphodynamic response in the shoreline position, largely controlled by human intervention, resulted in a long-term prevalent shoreline advance. This aspect is more evident in the residual signals (Fig. 7 for the M_1; see Supplementary Materials for the other macrocells), after removing both the influence of RSL and the oscillatory modes. These signals represent the magnitude of the overall trend driven by local morphodynamics, with non-linearities strictly associated with modifications occurring within the system, whether at the scale of a single cell or an entire macrocell. As explained above and shown in Figs. 6–7 (and in all Supplementary figures), there is evidence that nourishments and sediment extractions have driven long-term shoreline changes, often interacting with the effects of hard structures. This interplay complicates the direct estimation of these two distinct

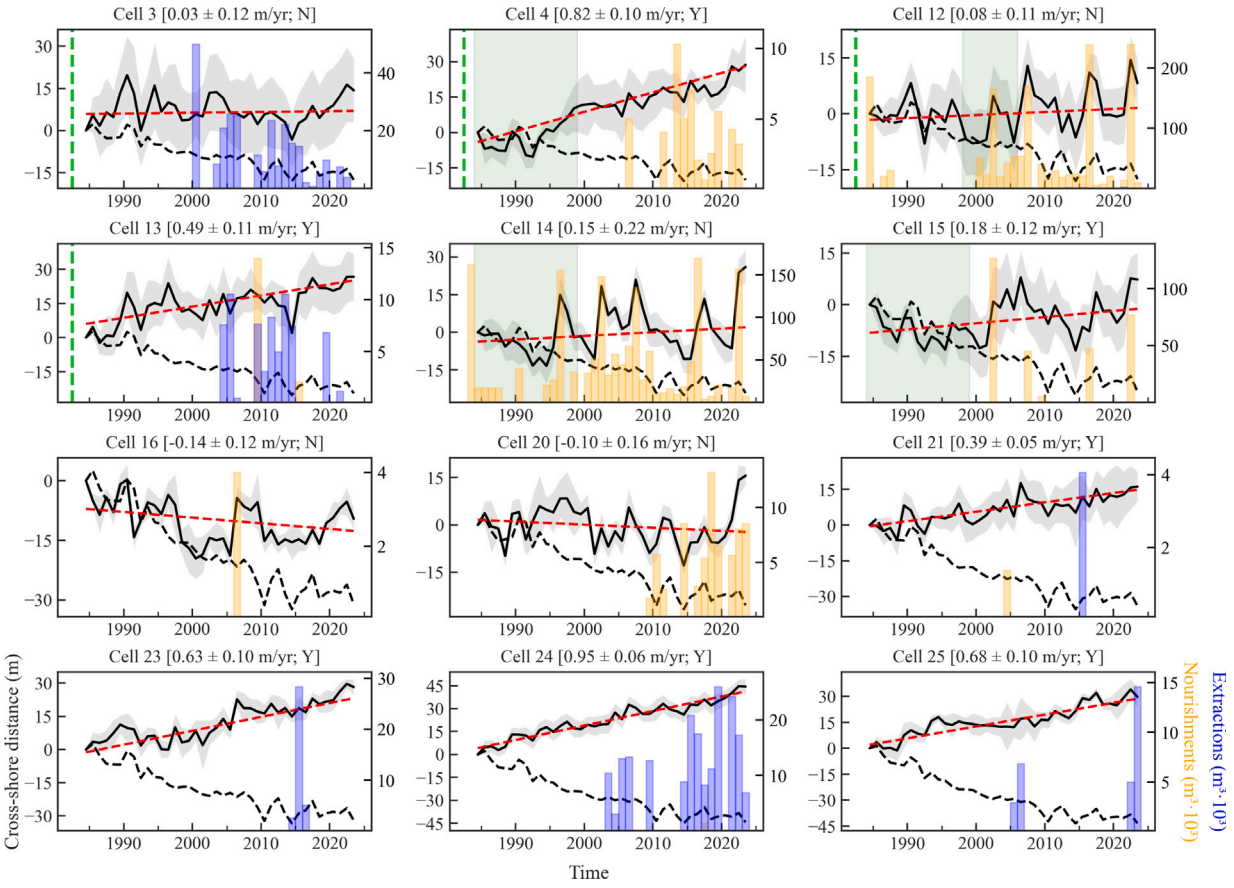

Fig. 6. The solid black line represents the annual averaged shoreline position for each specific cell within the M_1, along with its associated 1σ uncertainty (gray shaded area) and the linear trend (red hatched line) over the 40-year period. The trend value and its related error are stated above the corresponding subplot, while Y/N indicate whether the trend is statistically significant or not. The black hatched line indicates the theoretical shoreline evolution for each cell, estimated considering only the RSL change (see Section 3.3). Both observed and theoretical shoreline positions are shown in meters of displacement (left y-axis) with respect to the 1984 average, which is set to zero. Positive (negative) values indicate a shift seaward (landward), corresponding to shoreline progradation (erosion) within a cell. Orange and blue bars indicate the occurrence of sediment nourishment and extraction activities, respectively, for each specific cell and year. Nourishment and extraction volumes (data provided by Arpae) are expressed in $m^3 \times 10^3$ (refer to the right y-axis). Vertical green hatched lines indicate the placement of a new hard defense structure within a specific cell, while green-shaded areas denote the time range when the exact year of placement/re-adaptation is unknown. A green hatched line at 1982 signifies that hard structures were already in place before 1984.

anthropogenic influences, as they frequently occur simultaneously over the years. Furthermore, since most hard structures were placed before 1984, their impact on shoreline evolution is difficult to isolate. However, in certain cases (cells 4, 15, 31, 73, 75, 88, 90, and 91), the placement of hard structures during the 40-year period, combined with the absence of local sediment nourishment or extraction, allows for the attribution of the observed shoreline stabilization primarily to these structures.

It is interesting to note that some cells exhibit morphodynamic non-linearity even in the absence of new hard structure placements or local significant nourishment/extraction interventions. These variations are indirectly influenced by modifications in adjacent cells, with time-lagged effects propagating alongshore through the natural redistribution of sediments (e.g., cells 16 and 20). However, the interannual variability of natural origin is more difficult to ascertain, considering that, in this analysis, the effect of high-frequency processes has been virtually removed from annually averaged shorelines, as well as the seasonal behavior of the shoreline (Section 4.1). Nevertheless, climate-driven effects may be present at the multi-decadal scale, influencing shoreline interannual variability because, in addition to sea-level rise, changes in coastal hydrodynamics due to variations in the incident wave conditions and storminess are possibly correlated with climatic indices (Dodet et al., 2019). However, these effects can be more confidently recognized on open beaches (see, for instance, Castelle et al. (2021)) than along the ER coast, where hydrodynamics is largely partitioned due to many structures intercepting and disrupting the longshore current/drift.

5. Discussion

The analysis of an annually averaged shoreline position must be approached with caution, as these sand–water limits do not represent an actual boundary between land and sea. Indeed, the exact position of the shoreline at a specific location varies substantially over time and at very high frequencies (Boak and Turner, 2005), driven by the interplay of several processes of both anthropogenic and natural origin (as delineated in Section 2). Then, a reconstructed shoreline for a specific year in this analysis may not perfectly match an aerial image of the coast from the same year. This discrepancy occurs because the position of the sand–water limit interface, visible in the image, is tied to that particular moment in time. Indeed, such a comparison lacks meaning, as any instantaneous shoreline mapped from images should not be considered an averaged or "normal" condition of the beach, since such an interpretation represents one of the most misleading assumptions (Smith and Zarillo, 1990). Moreover, despite the very high resolution of aerial images, typically around 0.5 m and as high as 0.2 m in recent years, the manual mapping process can be highly subjective, varying significantly between observers (Crowell et al., 1991). This also

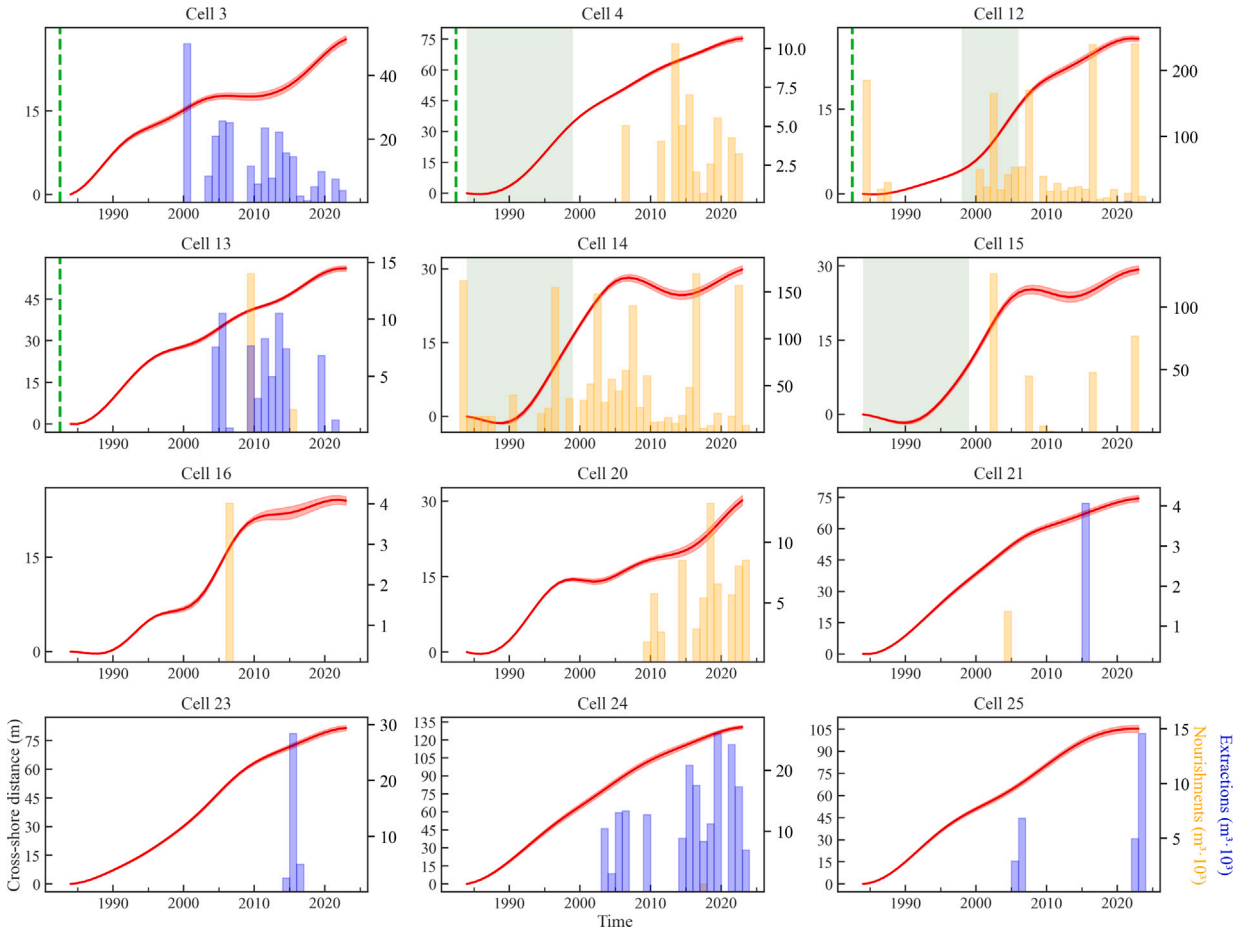

Fig. 7. The solid red line represents the residual, non-linear shoreline behavior of cells within M_1 over the period 1984–2023, after removing the RSL contribution and oscillatory modes, with its associated 1σ uncertainty (red shaded area). As in Fig. 6, the left y-axis indicates meters of displacement (relative to 1984), while the right y-axis refers to volumes ($m^3 \times 10^3$) of nourished/extracted sediment. The presence of hard defense structures within a cell is marked by a green hatched vertical line when the exact placement year is known or by a green shaded area when the onset is uncertain.

arises from the challenge of defining the sand–water limit, particularly on low slope beaches where wet sand can show different gray tones depending on the water content. Indeed, in the context of this study, the application of corrections (see Section 3.3) should not be viewed merely as a reduction of bias to detect the most likely exact position of the instantaneous shoreline, but rather as the removal of the influence of the high-frequency components from the analysis of shoreline changes. Thus, the correction and time-averaging adopted in this study provided averaged shoreline positions with short-term fluctuations and momentary run-up effects largely removed (Lippmann and Holman, 1989), strengthening the analysis of temporal evolution. This emphasis on hydrodynamic corrections aligns with evidence that SDS accuracy is strongly controlled by beach state. Thus, site-specific parametrization reduces uncertainty, whereas one-size-fits-all approaches may yield misleading conclusions (Konstantinou et al., 2023).

An interesting aspect of the long-term behavior of the reconstructed annual averaged shoreline position is that most of the observed cells exhibit either a progradational or stable pattern, as noted by Sytnik et al. (2018), despite the broader context of the ER coast, which is subject to persistent sea-level rise and significant subsidence. This condition might favor coastal retreat and beach migration landward, as indicated by the theoretical shoreline evolution estimated for each cell under the influence of RSL variations. Considering the low gradient of the ER coast, this would result in an estimated shoreline retreat of several tens of meters during the considered periods (Fig. 6 and Figs. S1-S5).

However, the large-scale behavior of a coastal system can evolve differently through dynamic responses to multiple interacting factors (Brunel et al., 2014; Castelle et al., 2018), or, as in the case of the ER coast, due to pervasive anthropogenic influence through multiple mechanisms. Indeed, widespread urbanization, the presence of hard structures, and human interventions aimed at preserving the status quo (Robert et al., 2023) have resulted in a general divergence in the evolution of each coastal cell, while also severely compromising coastal resilience through an overall stiffening of the system. Thus, beyond the cells experiencing substantial progradation (driven by alongshore sediment redistribution and the presence of long piers acting as barriers at the edge of some macrocells), the trends observed in most cells reflect the persistent anthropogenic effort to implement a 'hold the line' approach. This strategy ultimately masks the strong erosional trend that would have otherwise affected nearly the entire coastline if not counteracted by defensive measures and sufficient sediment input. Indeed, fluvial sources nowadays provide a limited sediment supply, as indicated by the fact that the observed average shoreline retreat near river mouths (e.g., cells 73–75, 93–97) is more intense than theoretically expected.

In this context, the absence of statistically significant trends across several cells (Figs. 6 and S1-S5) likely reflects the effect of anthropogenic interventions, which temporarily counteract retreat or progradation without stabilizing long-term trends; as a result, statistically flat trajectories locally prevail over significant erosion or accretion. Conversely, the two extremes observed within macrocell M_5 are connected as a result of the same process: the sediments provided by the Reno

River and originally deposited in the deltaic area (cells 93 to 96) tend to be redistributed northward by longshore currents (Aguzzi et al., 2016, 2020), eventually accumulating downdrift at the edge of M_5 (cells 98 and 100). Indeed, the Reno River Delta area, after a phase of progradation linked to sustained sediment supply in the early 20th century (Bondesan et al., 1978), entered a phase of progressive erosion in the late 1930s due to several anthropogenic factors, which led to drastic accelerations of erosion in the 1950s and 1980s (Preciso et al., 2012; Meli and Romagnoli, 2022).

Based on the annual time series described above, the use of satellite-derived data proved to be an efficient, cost-effective tool for monitoring shoreline evolution, with implications for coastal management and conservation (Tsai, 2024). Among the various applications of SDS-derived time series, both at the scale of individual coastal cells and broader spatial extents, is the ability to disentangle the different factors influencing coastal evolution. For instance, as demonstrated in this study, the combined effect of subsidence and sea-level change can be estimated and removed to isolate the contribution of morphodynamic processes, which in this case represents the residual signal. Additionally, anthropogenic influences on a given coastal sector can be assessed through time-series analysis. As shown in Fig. 6, nourishments and sediment extractions often manifest as abrupt shifts in shoreline position or, in some cases, a sawtooth pattern over time, particularly when interventions are periodic and substantial. Furthermore, knowledge of past nourishment and extraction activities may be incomplete or unavailable for certain shorelines worldwide (as is the case for some interventions along the ER coast, as stated in Section 3.3). In such instances, this approach could help identify and map these occurrences, as abrupt shifts or segmented evolution, particularly when absent in adjacent coastal tracts, can often be attributed to human influence.

Applying the same time-series diagnostics, the influence of hard structures can also be assessed, as these anthropogenic modifications alter the long-term tendency of a coastal tract, sometimes with a time lag that makes their impacts evident only after years. Therefore, multi-year analyses are essential for their identification (Tsai, 2024). As observed in some ER coastal cells, the introduction of new hard defense structures, or multiple additions over time, can significantly impact shoreline evolution and may result in the artificial stabilization of the shoreline, despite not resolving the causative factors of erosion. However, localized reversed or worsening erosional trends have been observed in several coastal sectors, some of which remain in a critical state, suggesting that current interventions are already insufficient or will soon become inadequate, particularly under climate-driven scenarios (Toimil et al., 2017). This underscores the need for sustainable adaptation strategies to enhance the resilience of coastlines against future climatic and environmental challenges (Hinkel et al., 2014).

From a management perspective, these dynamics entail significant socioeconomic exposure and planning needs for the ER coast. The area heavily relies on tourism, industry, and agriculture; therefore, both economic and social impacts are expected to be significant (Joint Research Centre, 2017), as approximately 15% to 40% of the ER shoreline is projected to be permanently submerged by 2050 and 2100, respectively (Celata and Gioia, 2024). However, the widespread reluctance of coastal populations to accept managed retreat Celata and Gioia (2024), Loizidou et al. (2024) may lead to the continued implementation of protective measures by stakeholders, preventing a shift towards different solutions, such as restoring natural habitats (Nordstrom et al., 2015), which could create a buffer zone. Similar to other worldwide sites, the need to balance sustainable environmental management and socio-economic issues requires the adoption of an integrated coastal management approach (Regione Emilia–Romagna, 2022).

6. Conclusions

In this study, the reconstructed yearly SDS positions along the ER coast over 1984–2023 indicate variable patterns and rates across coastal sectors (cells and macrocells) due to diverse interacting processes, site-specific settings, and individual characteristics. This variability is largely driven by widespread anthropogenic influences, including altered coastal dynamics from engineering defense structures, high-rate subsidence superimposed on natural processes, sediment supply from large-scale nourishments, and small-scale sediment extractions and redistribution. The approach employed here helps to mitigate complexities that would otherwise be difficult to address using conventional techniques. Although the application of corrections and annual averaging results in spatial smoothing, this approach also provides a solid basis for analyzing long-term shoreline evolution, for the first time here as a continuous time series. After signal processing and corrections to remove high-frequency components, the reconstructed time series of yearly averaged SDSs along the ER littoral provide a dataset suitable for assessing coastline evolution over the 40-year period. Overall, the main results, while consistent with previous studies using different techniques, provide new insights into coastal dynamics across multiple spatial and temporal scales along the ER coast. Despite the detailed parceling employed to distinguish tracts with specific dynamics, significant spatial and temporal variability persists in some areas, highlighting the complexity of shoreline evolution.

The resulting dataset constitutes one of the most temporally extensive records for the Emilia-Romagna coast, supports the evaluation of the interplay between natural processes and anthropogenic interventions across multiple scales, and provides a practical baseline for continued monitoring and adaptive coastal management. Nevertheless, limitations in the approach remain. Indeed, yearly averaging and the applied corrections reduce temporal uncertainty but introduce spatial smoothing that may mask short-term and small-scale variability. Moreover, the application of appropriate corrections to remove high-frequency influences may not be feasible everywhere along global coastlines, as the required datasets are not always available. Future work should integrate SDS with higher-resolution datasets and further refine hydrodynamic and topographic corrections to better capture localized dynamics. In addition, coupling the time-series dataset with sediment-budget assessments and local hydrodynamics could lead to new insights into coastal processes. Furthermore, since the approach detailed in this study is transferable to other coasts, using local observations (when available) and/or models to build appropriate corrections, insights into shoreline evolution and local history can be obtained even where in situ historical data are lacking. Under these conditions, SDS-based annual means from 1984 onward can resolve interannual to multidecadal variability and event-aligned responses (e.g., nourishments, extractions, structural changes, natural shifts), providing a valid decision-support baseline.

CRediT authorship contribution statement

Matteo Meli: Writing – review & editing, Writing – original draft, Visualization, Methodology, Investigation, Formal analysis. **Enrica Vecchi:** Writing – review & editing, Writing – original draft, Methodology, Investigation, Conceptualization. **Claudia Romagnoli:** Writing – review & editing, Writing – original draft, Supervision.

Declaration of competing interest

The authors declare that they have no known competing financial interests or personal relationships that could have appeared to influence the work reported in this paper.

Acknowledgments

The authors would like to thank Nunzio De Nigris and Flavia Sistilli from ARPAE for kindly providing access to the topobathymetric datasets and the nourishment/extraction database. We sincerely thank Kilian Vos for his prompt and insightful support through the official

discussion forum, which greatly facilitated our use of the CoastSat toolbox in this study. The authors would also like to thank three anonymous reviewers for their useful suggestions on earlier versions of this manuscript. This study was carried out within the RETURN Extended Partnership and received funding from the European Union Next–GenerationEU (National Recovery and Resilience Plan – NRRP, Mission 4, Component 2, Investment 1.3 – D.D. 1243 2/8/2022, PE0000005).

Appendix A. Supplementary data

Supplementary material related to this article can be found online at https://doi.org/10.1016/j.margeo.2025.107679.

Data availability

The main outcome products from this work are accessible at https://doi.org/10.5281/zenodo.14849128.

References

Aguzzi, M., Bonsignore, F., De Nigris, N., Morelli, M., Paccagnella, T., Romagnoli, C., Unguendoli, S., 2016. Stato del litorale Emiliano–Romagnolo al 2012. Erosione e interventi di difesa. I quaderni di Arpae, Bologna, Italy, p. 227.

Aguzzi, M., Costantino, R., De Nigris, N., Morelli, M., Romagnoli, C., Unguendoli, S., Vecchi, E., 2020. Stato del litorale Emiliano–Romagnolo al 2018. Erosione e interventi di difesa. I quaderni di Arpae, Bologna, Italy, p. 224.

Alexandrakis, G., Manasakis, C., Kampanis, N.A., 2015. Valuating the effects of beach erosion to tourism revenue. A management perspective. Ocean & Coastal Management 111, 1–11. http://dx.doi.org/10.1016/j.ocecoaman.2015.04.001.

Almar, R., Boucharel, J., Graffin, M., Abessolo, G.O., Thoumyre, G., Papa, F., Ranasinghe, R., Montano, J., Bergsma, E.W.J., Baba, M.W., Jin, F.F., 2023. Influence of El Niño on the variability of global shoreline position. Nat. Commun. 14, http://dx.doi.org/10.1038/s41467-023-38742-9.

Almonacid-Caballer, J., Sánchez-García, E., Pardo-Pascual, J.E., Balaguer-Beser, A.A., Palomar-Vázquez, J., 2016. Evaluation of annual mean shoreline position deduced from landsat imagery as a mid-term coastal evolution indicator. Mar. Geol. 372, 79–88. http://dx.doi.org/10.1016/j.margeo.2015.12.015.

Amorosi, A., Colalongo, M., Fiorini, F., Fusco, F., Pasini, G., Vaiani, S., Sarti, G., 2004. Palaeogeographic and palaeoclimatic evolution of the Po Plain from 150-ky core records. Glob. Planet. Change 40, 55–78. http://dx.doi.org/10.1016/S0921-8181(03)00098-5.

Arkema, K.K., Guannel, G., Verutes, G., Wood, S.A., Guerry, A., Ruckelshaus, M., Kareiva, P., Lacayo, M., Silver, J.M., 2013. Coastal habitats shield people and property from sea-level rise and storms. Nat. Clim. Chang. 3, 913–918. http://dx.doi.org/10.1038/nclimate1944.

Armaroli, C., Ciavola, P., Perini, L., Calabrese, L., Lorito, S., Valentini, A., Masina, M., 2012. Critical storm thresholds for significant morphological changes and damage along the Emilia-Romagna coastline, Italy. Geomorphology 143–144, 34–51. http://dx.doi.org/10.1016/j.geomorph.2011.09.006.

ARPA, 2002. Stato del litorale Emiliano–Romagnolo all'anno 2000. I quaderni di ARPA.

Aschenneller, B., Rietbroek, R., van der Wal, D., 2024. Changing sea level, changing shorelines: integration of remote–sensing observations at the Terschelling barrier island. Nat. Hazards Earth Syst. Sci. 24 (11), 4145–4177. http://dx.doi.org/10.5194/nhess-24-4145-2024.

Athanasiou, P., van Dongeren, A., Giardino, A., Vousdoukas, M., Gaytan-Aguilar, S., Ranasinghe, R., 2019. Global distribution of nearshore slopes with implications for coastal retreat. Earth Syst. Sci. Data 11 (4), 1515–1529, https://essd.copernicus.org/articles/11/1515/2019/.

Barnard, P.L., Foxgrover, A., Hart, J.F., O'Neill, P.L.A., van Ormondt, M., Vitousek, S., Wood, N., Hayden Mand Jones, J., 2019. Dynamic flood modeling essential to assess the coastal impacts of climate change. Sci. Rep. 9, 4309. http://dx.doi.org/10.1038/s41598-019-40742-z.

Battjes, J., 1974. Surf Similarity. In: Proceedings of the 14th Conference of Coastal Engineering. ASCE, pp. 466–480. http://dx.doi.org/10.1061/9780872621138.029.

Bishop-Taylor, R., Nanson, R., Sagar, S., Lymburner, L., 2021. Mapping Australia's dynamic coastline at mean sea level using three decades of Landsat imagery. Remote Sens. Environ. 267, 112734. http://dx.doi.org/10.1016/j.rse.2021.112734.

Bishop-Taylor, R., Sagar, S., Lymburner, L., Alam, I., Sixsmith, J., 2019. Sub–pixel waterline extraction: Characterising accuracy and sensitivity to indices and spectra. Remote. Sens. 11 (24), http://dx.doi.org/10.3390/rs11242984.

Bitelli, G., Bonsignore, F., Unguendoli, M., 2000. Levelling and GPS networks to monitor ground subsidence in the Southern Po Valley. J. Geodyn. 30 (3), 355–369. http://dx.doi.org/10.1016/S0264-3707(99)00071-X.

Boak, E.H., Turner, I.L., 2005. Shoreline definition and detection: A review. J. Coast. Res. 214, 688–703. http://dx.doi.org/10.2112/03-0071.1.

Bondesan, M., Calderoni, G., Cin, R.D., 1978. Il litorale delle province di Ferrara e di Ravenna (Alto Adriatico); evoluzione morfologica e distribuzione dei sedimenti. Boll. Della Soc. Geol. Ital. 97, 247–287.

Brown, S., O'Dea, A., Conery, I., Brodie, K., 2025. Assessing shorelines extracted from satellite imagery using coincident terrestrial lidar linescans. Coast. Eng. 199, 104718. http://dx.doi.org/10.1016/j.coastaleng.2025.104718.

Brunel, C., Certain, R., Sabatier, F., Robin, N., Barusseau, J., Aleman, N., Raynal, O., 2014. 20th century sediment budget trends on the Western Gulf of Lions shoreface (France): An application of an integrated method for the study of sediment coastal reservoirs. Geomorphology 204, 625–637. http://dx.doi.org/10.1016/j.geomorph.2013.09.009.

Bruno, L., Campo, B., Costagli, B., Stouthamer, E., Teatini, P., Zoccarato, C., Amorosi, A., 2020. Factors controlling natural subsidence in the Po Plain. Proc. Int. Assoc. Hydrol. Sci. 382, 285–290. http://dx.doi.org/10.5194/piahs-382-285-2020.

Bruno, L., Meli, M., Garberi, M.L., 2024. Human–induced landscape modification in the in the last two centuries in the Po delta plain (Northern Italy). Anthropocene 48, 100453. http://dx.doi.org/10.1016/j.ancene.2024.100453.

Calabrese, L., Correggiari, A., Perini, L., Remia, A., 2024. La Geologia tra la Terra e il Mare. Strumenti per la gestione dei rischi costieri in Emilia–Romagna. Centro Stampa Regione Emilia–Romagna, http://dx.doi.org/10.5281/zenodo.10810185.

Carminati, E., Di Donato, G., 1999. Separating natural and anthropogenic vertical movements in fast subsiding areas: The Po Plain (N. Italy) Case. Geophys. Res. Lett. 26 (15), 2291–2294. http://dx.doi.org/10.1029/1999GL900518.

Carminati, E., Martinelli, G., 2002. Subsidence rates in the Po Plain, northern Italy: the relative impact of natural and anthropogenic causation. Eng. Geol. 66 (3), 241–255. http://dx.doi.org/10.1016/S0013-7952(02)00031-5.

Castelle, B., Guillot, B., Marieu, V., Chaumillon, E., Hanquiez, V., Bujan, S., Poppeschi, C., 2018. Spatial and temporal patterns of shoreline change of a 280–km high–energy disrupted sandy coast from 1950 to 2014: SW France. Estuar. Coast. Shelf Sci. 200, 212–223. http://dx.doi.org/10.1016/j.ecss.2017.11.005.

Castelle, B., Kras, E., Masselink, G., Scott, T., Konstantinou, A., Luijendijk, A., 2024. Satellite-derived sandy shoreline trends and interannual variability along the Atlantic coast of Europe. Sci. Rep. 14, 13002. http://dx.doi.org/10.1038/s41598-024-63849-4.

Castelle, B., Masselink, G., 2023. Morphodynamics of wave-dominated beaches. Camb. Prism.: Coast. Futur. 1, e1. http://dx.doi.org/10.1017/cft.2022.2.

Castelle, B., Masselink, G., Scott, T., Stokes, C., Konstantinou, A., Marieu, V., Bujan, S., 2021. Satellite–derived shoreline detection at a high–energy meso–macrotidal beach. Geomorphology 383, 107707. http://dx.doi.org/10.1016/j.geomorph.2021.107707.

Celata, F., Gioia, E., 2024. Resist or retreat? Beach erosion and the climate crisis in Italy: Scenarios, impacts and challenges. Appl. Geogr. 169, 103335. http://dx.doi.org/10.1016/j.apgeog.2024.103335.

Ciavola, P., Armaroli, C., Chiggiato, J., Valentini, A., Deserti, M., Perini, L., Luciani, P., 2007. Impact of storms along the coastline of Emilia-Romagna: the morphological signature on the Ravenna coastline (Italy). J. Coast. Res. 50 (sp1), 540. http://dx.doi.org/10.2112/JCR-SI50-103.1.

Cipolletti, M.P., Delrieux, C.A., Perillo, G.M.E., Cintia Piccolo, M., 2012. Superresolution border segmentation and measurement in remote sensing images. Comput. Geosci. 40, 87–96. http://dx.doi.org/10.1016/j.cageo.2011.07.015.

Codiga, D.L., 2011. Unified Tidal Analysis and Prediction Using the UTide Matlab Functions. Technical Report 2011–01, Graduate School of Oceanography, University of Rhode Island, Narragansett, RI, URL ftp://www.po.gso.uri.edu/pub/downloads/codiga/pubs/2011Codiga-UTide-Report.pdf.

Correggiari, A.M., Roveri, M., Trincardi, F., 1996. Late Pleistocene and Holocene evolution of the North Adriatic Sea. Ital. J. Quat. Sci. 9, 697–704.

Crowell, M., Leatherman, S.P., Buckley, M.K., 1991. Historical shoreline change: Error analysis and mapping accuracy. J. Coast. Res. 7, 839–852, https://www.jstor.org/stable/4297899.

Cuttler, M.V.W., Vos, K., Branson, P., Hansen, J.E., O'Leary, M., Browne, N.K., Lowe, R.J., 2020. Interannual response of Reef islands to climate–driven variations in water level and wave climate. Remote. Sens. 12 (24), 4089. http://dx.doi.org/10.3390/rs12244089.

Davies, J., 1964. A morphogenic approach to world shorelines. Z. Für Geomorphol. 8, 127–142. http://dx.doi.org/10.1127/zfg/mortensen/8/1964/127.

Delaunay, B., 1934. Sur la sphere vide. Bull. de L'Academie Des Sci. de L'URSS. Cl. Des Sci. Math. et Nat. 6, 793–800.

Devlin, A.T., Pan, J., Lin, H., 2019. Tidal variability in the Hong Kong region. Ocean. Sci. 15 (4), 853–864. http://dx.doi.org/10.5194/os-15-853-2019.

Di Luccio, D., Benassai, G., Budillon, G., Mucerino, L., Montella, R., Pugliese Carratelli, E., 2018. Wave run–up prediction and observation in a micro–tidal beach. Nat. Hazards Earth Syst. Sci. 18 (11), 2841–2857. http://dx.doi.org/10.5194/nhess-18-2841-2018.

Dodet, G., Bertin, X., Bouchette, F., Gravelle, M., Testut, L., Wöppelmann, G., 2019. Characterization of sea-level variations along the Metropolitan Coasts of France: Waves, tides, storm surges and long-term changes. J. Coast. Res. 88 (sp1), 10–24. http://dx.doi.org/10.2112/SI88-003.1.

Egbert, G.D., Erofeeva, S.Y., 2002. Efficient inverse modeling of barotropic ocean tides. J. Atmos. Ocean. Technol. 19 (2), 183–204. http://dx.doi.org/10.1175/1520-0426(2002)019<0183:EIMOBO>2.0.CO;2.

Gambolati, G., Teatini, P., 1998. Numerical analysis of land subsidence due to natural compaction of the upper Adriatic sea basin. In: Gambolati, G. (Ed.), CENAS: Coastline Evolution of the Upper Adriatic Sea Due To Sea Level Rise and Natural and Anthropogenic Land Subsidence. Springer Netherlands, Dordrecht, The Netherlands, pp. 103–131. http://dx.doi.org/10.1007/978-94-011-5147-4_5.

García-Rubio, G., Huntley, D., Russell, P., 2015. Evaluating shoreline identification using optical satellite images. Mar. Geol. 359, 96–105. http://dx.doi.org/10.1016/j.margeo.2014.11.002.

Ghermandi, A., Nunes, P.A.L.D., 2013. A global map of coastal recreation values: Results from a spatially explicit meta-analysis. Ecol. Econom. 86, 1–15. http://dx.doi.org/10.1016/j.ecolecon.2012.11.006.

Gómez-Pazo, A., Payo, A., Paz-Delgado, M.V., Delgadillo-Calzadilla, M.A., 2022. Open digital shoreline analysis system: ODSAS v1.0. J. Mar. Sci. Eng. 10 (1), 26. http://dx.doi.org/10.3390/jmse10010026.

Gorelick, N., Hancher, M., Dixon, M., Ilyushchenko, S., Thau, D., Moore, R., 2017. Google Earth Engine: Planetary–scale geospatial analysis for everyone. Remote Sens. Environ. 202, 18–27. http://dx.doi.org/10.1016/j.rse.2017.06.031.

Gregory, J.M., Griffies, S.M., Hughes, C.W., Lowe, J.A., Church, J.A., Fukimori, I., Gomez, N., Kopp, R., Landered, F., Cozannet, G.L., Ponte, R.M., Stammer, D., Tamisiea, M.E., van de Wal, R.S.W., 2019. Concepts and terminology for sea level: Mean, variability and change, both local and global. Surv. Geophys. 40, 1251–1289. http://dx.doi.org/10.1007/s10712-019-09525-z.

Hagenaars, G., de Vries, S., Luijendijk, A.P., de Boer, W.P., Reniers, A.J., 2018. On the accuracy of automated shoreline detection derived from satellite imagery: A case study of the sand motor mega–scale nourishment. Coast. Eng. 133, 113–125. http://dx.doi.org/10.1016/j.coastaleng.2017.12.011.

Haigh, I.D., Marcos, M., Talke, S.A., Woodworth, P.L., Hunter, J.R., Hague, B., Arns, A., Bradshaw, E., Thompson, P., 2023. GESLA Version 3: A major update to the global higher–frequency sea-level dataset. Geosci. Data J. 10 (3), 293–314. http://dx.doi.org/10.1002/gdj3.174.

Hamed, K.H., Ramachandra Rao, A., 1998. A modified Mann–Kendall trend test for autocorrelated data. J. Hydrol. 204 (1), 182–196. http://dx.doi.org/10.1016/S0022-1694(97)00125-X.

Hersbach, H., Bell, B., Berrisford, P., Hirahara, S., Horányi, A., Muñoz-Sabater, J., Nicolas, J., Peubey, C., Radu, R., Schepers, D., Simmons, A., Soci, C., Abdalla, S., Abellan, X., Balsamo, G., Bechtold, P., Biavati, G., Bidlot, J., Bonavita, M., De Chiara, G., Dahlgren, P., Dee, D., Diamantakis, M., Dragani, R., Flemming, J., Forbes, R., Fuentes, M., Geer, A., Haimberger, L., Healy, S., Hogan, R.J., Hólm, E., Janisková, M., Keeley, S., Laloyaux, P., Lopez, P., Lupu, C., Radnoti, G., de Rosnay, P., Rozum, I., Vamborg, F., Villaume, S., Thépaut, J.-N., 2020. The ERA5 global reanalysis. Q. J. R. Meteorol. Soc. 146 (730), 1999–2049. http://dx.doi.org/10.1002/qj.3803.

Himmelstoss, E.A., Henderson, R.E., Farris, A.S., Kratzmann, M.G., Bartlett, M.K., Ergul, A., McAndrews, J., Cibaj, R., Zichichi, J.L., Thieler, E.R., 2024. Digital Shoreline Analysis System version 6.0: U.S. Geological Survey software release. Technical Report, USGS, http://dx.doi.org/10.5066/P13WIZ8M.

Hinkel, J., Lincke, D., Vafeidis, A.T., Perrette, M., Nicholls, R.J., Tol, R.S.J., Marzeion, B., Fettweis, X., Ionescu, C., Levermann, A., 2014. Coastal flood damage and adaptation costs under 21st century sea-level rise. Proc. Natl. Acad. Sci. 111 (9), 3292–3297. http://dx.doi.org/10.1073/pnas.1222469111.

IDROSER, 1983. Il trasporto solido fluviale nei bacini tributari dell'Adriatico. Regione Emilia–Romagna, Piano progettuale per la difesa della costa Emiliano–Romagnola. Regione Emilia–Romagna, Bologna, Italy, p. 429.

IDROSER, 1996. Progetto di Piano per la Difesa dal Mare e la Riqualificazione Ambientale del Litorale della Regione Emilia–Romagna, Relazione Generale. Regione Emilia–Romagna, Bologna, Italy, p. 365.

IPCC, 2023. Ocean, cryosphere and sea level change. In: Climate Change 2021 - The Physical Science Basis: Working Group I Contribution to the Sixth Assessment Report of the Intergovernmental Panel on Climate Change. Cambridge University Press, pp. 1211–1362. http://dx.doi.org/10.1017/9781009157896.011.

Joint Research Centre, 2017. Climate Change and Critical Infrastructure – Flood. Publications Office of the European Union.

Konlechner, T.M., Kennedy, D.M., O'Grady, J.J., Leach, C., Ranasinghe, R., Carvalho, R.C., Luijendijk, A.P., McInnes, K.L., Ierodiaconou, D., 2020. Mapping spatial variability in shoreline change hotspots from satellite data; a case study in southeast Australia. Estuar. Coast. Shelf Sci. 246, 107018. http://dx.doi.org/10.1016/j.ecss.2020.107018.

Konstantinou, A., Scott, T., Masselink, G., Stokes, K., Conley, D., Castelle, B., 2023. Satellite-based shoreline detection along high-energy macrotidal coasts and influence of beach state. Mar. Geol. 462, 107082. http://dx.doi.org/10.1016/j.margeo.2023.107082.

Lionello, P., Cavaleri, L., Nissen, K., Pino, C., Raicich, F., Ulbrich, U., 2012. Severe marine storms in the Northern Adriatic: Characteristics and trends. Phys. Chem. Earth, Parts A/B/C 40–41, 93–105. http://dx.doi.org/10.1016/j.pce.2010.10.002.

Lippmann, T., Holman, R., 1989. Quantification of sand bar morphology: A video technique based on wave dissipation. J. Geophys. Res. 94, 995–1011. http://dx.doi.org/10.1029/JC094iC01p00995.

Loizidou, X.I., Orthodoxou, D.L., Loizides, M.I., Petsa, D., Anzidei, M., 2024. Adapting to sea level rise: participatory, solution-oriented policy tools in vulnerable Mediterranean areas. Environ. Syst. Decis. 44, 126–144. http://dx.doi.org/10.1007/s10669-023-09910-5.

Lorito, S., Calabrese, L., Perini, L., Cibin, U., 2010. Il sistema mare-costa dell'Emilia-Romagna. Pendragon, pp. 109–118.

Luijendijk, A., Hagenaars, G., Ranasinghe, R., Baart, F., Donchyts, G., Aarninkhof, S., 2018. The state of the world's beaches. Sci. Rep. 8, 1–11. http://dx.doi.org/10.1038/s41598-018-24630-6.

Lyard, F.H., Allain, D.J., Cancet, M., Carrère, L., Picot, N., 2021. FES2014 global ocean tide atlas: design and performance. Ocean. Sci. 17 (3), 615–649. http://dx.doi.org/10.5194/os-17-615-2021.

Marcaccio, M., Mazzei, M., 2023. Monitoraggio dei movimenti verticali del suolo e aggiornamento della cartografia di subsidenza nella pianura dell'Emilia–Romagna. Periodo 2016–2021. Technical Report, Regione Emilia–Romagna, Arpae Emilia–Romagna, Bologna, Italy, https://www.arpae.it/it/temi-ambientali/suolo/rapporti/rapporti-subsidenza/monitoraggio-movimenti-verticali-suolo-e-cartografia-subsidenza-emilia-romagna-2016-2021.zip/view. (Accessed 19 August 2024).

Martínez, M., Intralawan, A., Vázquez, G., Pérez-Maqueo, O., Sutton, P., Landgrave, R., 2007. The coasts of our world: Ecological, economic and social importance. Ecol. Econom. 63 (2), 254–272. http://dx.doi.org/10.1016/j.ecolecon.2006.10.022.

Masina, M., Ciavola, P., 2011. Analisi dei livelli marini estremi e delle acque alte lungo il litorale ravennate. Stud. Costieri 18, 87–101.

Meli, M., 2024. The potential recording of North Ionian Gyre's reversals as a decadal signal in sea level during the instrumental period. Sci. Rep. 14, 4907. http://dx.doi.org/10.1038/s41598-024-55579-4.

Meli, M., Camargo, C.M.L., Olivieri, M., Slangen, A.B.A., Romagnoli, C., 2023. Sea–level trend variability in the Mediterranean during the 1993–2019 period. Front. Mar. Sci. 10, 1150488. http://dx.doi.org/10.3389/fmars.2023.1150488.

Meli, M., Marcaccio, M., Mazzei, M., Romagnoli, C., 2025. Temporal and spatial analysis of relative sea-level changes across the Emilia-Romagna coastal plain (northern Adriatic Sea). Estuar. Coast. Shelf Sci. 314, 109143. http://dx.doi.org/10.1016/j.ecss.2025.109143.

Meli, M., Olivieri, M., Romagnoli, C., 2021. Sea–level change along the Emilia–Romagna Coast from tide gauge and satellite altimetry. Remote. Sens. 13, 97. http://dx.doi.org/10.3390/rs13010097.

Meli, M., Romagnoli, C., 2022. Evidence and implications of hydrological and climatic change in the reno and lamone river basins and Related Coastal Areas (Emilia–Romagna, Northern Italy) over the last century. Water 14, 2650. http://dx.doi.org/10.3390/w14172650.

Mentaschi, L., Vousdoukas, M.I., Pekel, J.F., Voukouvalas, E., Feyen, L., 2018. Global long-term observations of coastal erosion and accretion. Sci. Rep. 8, 1–11. http://dx.doi.org/10.1038/s41598-018-30904-w.

Muis, S., Apecechea, M.I., Dullaart, J., de Lima Rego, J., Madsen, K.S., Su, J., Yan, K., Verlaan, M., 2020. A high–resolution global dataset of extreme sea levels, tides, and storm surges, including future projections. Front. Mar. Sci. 7, http://dx.doi.org/10.3389/fmars.2020.00263.

Nordstrom, K.F., Armaroli, C., Jackson, N.L., Ciavola, P., 2015. Opportunities and constraints for managed retreat on exposed sandy shores: Examples from Emilia-Romagna, Italy. Ocean & Coastal Management 104, 11–21. http://dx.doi.org/10.1016/j.ocecoaman.2014.11.010.

Otsu, N., 1979. A threshold selection method from gray-level histograms. IEEE Trans. Syst. Man Cybern. 20, 62–66. http://dx.doi.org/10.1109/TSMC.1979.4310076.

Pan, H., Gan, M., Xu, T., Wei, Z., 2024. A century of tidal evolution around the Panama Canal. Cont. Shelf Res. 283, 105357. http://dx.doi.org/10.1016/j.csr.2024.105357.

Perini, L., Calabrese, L., Deserti, M., Valentini, A., Ciavola, P., Armaroli, C., 2011. Le mareggiate e gli impatti sulla costa in Emilia-Romagna. I Quaderni di Arpa, p. 144.

Perini, L., Calabrese, L., Salerno, G., Ciavola, P., Armaroli, C., 2016. Evaluation of coastal vulnerability to flooding: comparison of two different methods adopted by the Emilia–Romagna region (Italy). Nat. Hazards Earth Syst. Sci. 181–194. http://dx.doi.org/10.5194/nhess-16-181-2016.

Preciso, E., Salemi, E., Billi, P., 2012. Land use changes, torrent control works and sediment mining: effects on channel morphology and sediment flux, case study of the Reno River (Northern Italy). Hydrol. Process. 26 (8), 1134–1148. http://dx.doi.org/10.1002/hyp.8202.

Preti, M., Nigris, N.D., Morelli, M., Monti, M., Bonsignore, F., Aguzzi, M., 2009. Stato del litorale Emiliano–Romagnolo all'anno 2007 e piano decennale di gestione. I quaderni di Arpa, p. 272.

Ramos-Alcántara, J., Gomis, D., Jordà, G., 2022. Reconstruction of Mediterranean coastal sea level at different timescales based on tide gauge records. Ocean. Sci. 18 (6), 1781–1803. http://dx.doi.org/10.5194/os-18-1781-2022.

Regione Emilia–Romagna, 2014. Il sistema gestionale delle celle litoranee – Sicell. Aggiornamento 2006–2012. Centro Stampa Regione Emilia–Romagna, p. 78.

Regione Emilia–Romagna, 2022. Strategia di Gestione Integrata per la Difesa e l'Adattamento della Costa ai cambiamenti climatici (GIDAC). Centro Stampa Regione Emilia–Romagna, p. 285, URL https://ambiente.regione.emilia-romagna.it/it/suolo-bacino/argomenti/difesa-della-costa/gidac.

Robert, S., Quercy, A., Schleyer-Lindenmann, A., 2023. Territorial inertia versus adaptation to climate change. When local authorities discuss coastal management in a French Mediterranean region. Glob. Environ. Chang. 81, 102702. http://dx.doi.org/10.1016/j.gloenvcha.2023.102702.

Romagnoli, C., Sistilli, F., Cantelli, L., Aguzzi, M., De Nigris, N., Morelli, M., Gaeta, M.G., Archetti, R., 2021. Beach Monitoring and Morphological Response in the Presence of Coastal Defense Strategies at Riccione (Italy). J. Mar. Sci. Eng. 9 (8), http://dx.doi.org/10.3390/jmse9080851.

Schlacher, T.A., Dugan, J., Schoeman, D.S., Lastra, M., Jones, A., Scapini, F., McLachlan, A., Defeo, O., 2007. Sandy beaches at the brink. Diversity and Distributions 13 (5), 556–560. http://dx.doi.org/10.1111/j.1472-4642.2007.00363.x.

Sen, P.K., 1968. Estimates of the regression coefficient based on Kendall's Tau. J. Amer. Statist. Assoc. 63 (324), 1379–1389. http://dx.doi.org/10.1080/01621459.1968.10480934.

Smith, G.L., Zarillo, G.A., 1990. Calculating long–term shoreline recession rates using aerial photographic and beach profiling techniques. J. Coast. Res. 6, 111–120, https://www.jstor.org/stable/4297648.

Stockdon, H.F., Holman, R.A., Howd, P.A., Sallenger, A.H., 2006. Empirical parameterization of setup, swash, and runup. Coast. Eng. 53 (7), 573–588. http://dx.doi.org/10.1016/j.coastaleng.2005.12.005.

Sun, W., Zhou, X., Zhou, D., Sun, Y., 2022. Advances and accuracy assessment of ocean tide models in the antarctic ocean. Front. Earth Sci. 10, http://dx.doi.org/10.3389/feart.2022.757821.

Sytnik, O., Del Río, L., Greggio, N., Bonetti, J., 2018. Historical shoreline trend analysis and drivers of coastal change along the Ravenna coast, NE Adriatic. Environ. Earth Sci. 77 (23), 779. http://dx.doi.org/10.1007/s12665-018-7963-8.

Syvitski, J., Angel, J., Saito, Y., Overeem, I., Vörösmarty, C., Wang, H., Olago, D., 2022. Earth's sediment cycle during the anthropocene. Nat. Rev. Earth Environ. 3, 179–196. http://dx.doi.org/10.1038/s43017-021-00253-w.

Teatini, P., Ferronato, M., Gambolati, G., Gonella, M., 2006. Groundwater pumping and land subsidence in the Emilia–Romagna coastland, Italy: Modeling the past occurrence and the future trend. Water Resour. Res. 42 (1), http://dx.doi.org/10.1029/2005WR004242.

Teatini, P., Tosi, L., Strozzi, T., 2011. Quantitative evidence that compaction of Holocene sediments drives the present land subsidence of the Po Delta, Italy. J. Geophys. Res.: Solid Earth 116 (B8), http://dx.doi.org/10.1029/2010JB008122.

Toimil, A., Camus, P., Losada, I., Le Cozannet, G., Nicholls, R., Idier, D., Maspataud, A., 2020. Climate change–driven coastal erosion modelling in temperate sandy beaches: Methods and uncertainty treatment. Earth–Science Rev. 202, 103110. http://dx.doi.org/10.1016/j.earscirev.2020.103110.

Toimil, A., Losada, I.J., Camus, P., Díaz-Simal, P., 2017. Managing coastal erosion under climate change at the regional scale. Coast. Eng. 128, 106–122. http://dx.doi.org/10.1016/j.coastaleng.2017.08.004.

Tsai, Y.-L.S., 2024. Nation-scale multidecadal shoreline extraction and coastal spatio-temporal change monitoring using cross-mission remote sensing data. Ocean & Coastal Management 253, 107136. http://dx.doi.org/10.1016/j.ocecoaman.2024.107136.

Turner, I.L., Harley, M.D., Almar, R., Bergsma, E.W., 2021. Satellite optical imagery in coastal engineering. Coast. Eng. 167, 103919. http://dx.doi.org/10.1016/j.coastaleng.2021.103919.

Vecchi, E., 2023. Impact of Geomatic Techniques on Topo–Bathymetric Surveys for Coastal Analysis (Ph.D. thesis). Alma Mater Studiorum – University of Bologna, URL http://amsdottorato.unibo.it/10535/.

Vecchi, E., Tavasci, L., De Nigris, N., Gandolfi, S., 2021. GNSS and photogrammetric UAV derived data for coastal monitoring: A case of study in Emilia–Romagna, Italy. J. Mar. Sci. Eng. 9 (11), 1194. http://dx.doi.org/10.3390/jmse9111194.

Vitousek, S., Vos, K., Splinter, K.D., Erikson, L., Barnard, P.L., 2023. A model integrating satellite–derived shoreline observations for predicting fine–scale shoreline response to waves and sea–level rise across large coastal regions. Authorea Prepr. http://dx.doi.org/10.22541/essoar.167839941.16313003/v1.

Vos, K., Harley, M.D., Splinter, K.D., Simmons, J.A., Turner, I.L., 2019a. Sub–annual to multi–decadal shoreline variability from publicly available satellite imagery. Coast. Eng. 150, 160–174. http://dx.doi.org/10.1016/j.coastaleng.2019.04.004.

Vos, K., Harley, M.D., Splinter, K.D., Walker, A., Turner, I.L., 2020. Beach slopes from satellite-derived shorelines. Geophys. Res. Lett. 47 (14), http://dx.doi.org/10.1029/2020GL088365, e2020GL088365.

Vos, K., Harley, M.D., Turner, I.L., Splinter, K.D., 2023a. Pacific shoreline erosion and accretion patterns controlled by El Niño/Southern Oscillation. Nat. Geosci. 16, 140–146. http://dx.doi.org/10.1038/s41561-022-01117-8.

Vos, K., Splinter, K.D., Harley, M.D., Simmons, J.A., Turner, I.L., 2019b. CoastSat: A Google Earth Engine–enabled Python toolkit to extract shorelines from publicly available satellite imagery. Environ. Model. Softw. 122, 104528. http://dx.doi.org/10.1016/j.envsoft.2019.104528.

Vos, K., Splinter, K.D., Palomar-Vázquez, J., Pardo-Pascual, J.E., Almonacid-Caballer, J., Cabezas-Rabadán, C., Kras, E.C., Luijendijk, A.P., Calkoen, F., Almeida, L.P., Pais, D., Klein, A.H.F., Mao, Y., Harris, D., Castelle, B., Buscombe, D., Vitousek, S., 2023b. Benchmarking satellite–derived shoreline mapping algorithms. Commun. Earth Environ. 4, 345. http://dx.doi.org/10.1038/s43247-023-01001-2.

Wang, Q., Ma, Y., Cheng, Z., Du, Y., 2023. Coastline changes under natural and anthropogenic drivers in a macro–tidal estuary between 2000–2020. Front. Mar. Sci. 10, http://dx.doi.org/10.3389/fmars.2023.1335064.

Wu, Z., Huang, N.E., 2009. Ensemble Empirical Mode Decomposition: a noise–assisted data analysis method. Adv. Adapt. Data Anal. 01 (01), 1–41. http://dx.doi.org/10.1142/S1793536909000047.

Zerbini, S., Bruni, S., Raicich, F., 2021. Tide gauge data archaeology provides natural subsidence rates along the coasts of the Po Plain and of the Veneto–Friuli Plain, Italy. Geophys. J. Int. 225, 253–260. http://dx.doi.org/10.1093/gji/ggaa602.

Zhang, K.Q., Douglas, B.C., Leatherman, S.P., 2004. Global warming and coastal erosion. Clim. Change 64, 41–58. http://dx.doi.org/10.1023/b:clim.0000024690.32682.48.

Zhang, K., Zhang, F., Wan, W., Yu, H., Sun, J., Del Ser, J., Elyan, E., Hussain, A., 2023. Panchromatic and multispectral image fusion for remote sensing and earth observation: Concepts, taxonomy, literature review, evaluation methodologies and challenges ahead. Inf. Fusion 93, 227–242. http://dx.doi.org/10.1016/j.inffus.2022.12.026.

Zollini, S., Dominici, D., Alicandro, M., Cuevas-González, M., Angelats, E., Ribas, F., Simarro, G., 2023. New methodology for shoreline extraction using optical and radar (SAR) satellite imagery. J. Mar. Sci. Eng. 11 (3), http://dx.doi.org/10.3390/jmse11030627.